Juha-Matti Huusko
Yliopistokatu 7, 80100 Joensuu
juha-matti.huusko@uef.fi
+358 40 528 2815

Tehtävän kannalta merkittävät julkaisut

sivut 2-25

Gröhn, J., J-M. Huusko, J. Rättyä, Linear differential equations with slowly growing solutions, Trans. Amer. Math. Soc. 370 (2018), 7201-7227.

sivut 26-35

Pesonen, H.A., J.-M. Huusko, X. Zang, A.T. Friberg, J. Turunen and T. Setälä, Partial spectral and temporal coherence of plane-wave pulse trains in second-harmonic generation, J. Opt. (2021)

sivut 36-45

Pesonen, H., A. Halder, J.-M. Huusko, A.T. Friberg, T. Setälä and J. Turunen, Spatial coherence effects in second-harmonic generation of scalar light fields, Journal of Optics, Volume 23, Number 3.

LINEAR DIFFERENTIAL EQUATIONS WITH SLOWLY GROWING SOLUTIONS

JANNE GRÖHN, JUHA-MATTI HUUSKO AND JOUNI RÄTTYÄ

Abstract. This research concerns linear differential equations in the unit disc of the complex plane. In the higher order case the separation of zeros (of maximal multiplicity) of solutions is considered, while in the second order case slowly growing solutions in H^∞, BMOA and the Bloch space are discussed. A counterpart of the Hardy-Stein-Spencer formula for higher derivatives is proved, and then applied to study solutions in the Hardy spaces.

1. Introduction

A fundamental objective in the study of complex linear differential equations with analytic coefficients in a complex domain is to relate the growth of coefficients to the growth of solutions and to the distribution of their zeros. In the case of fast growing solutions, Nevanlinna and Wiman-Valiron theories have turned out to be very useful both in the unit disc [10, 24] and in the complex plane [23, 24].

We restrict ourselves to the case of the unit disc $\mathbb{D} = \{z \in \mathbb{C} : |z| < 1\}$. In addition to methods above, theory of conformal maps has been used to establish interrelationships between the growth of coefficients and the geometric distribution (and separation) of zeros of solutions. This connection was one of the highlights in Nehari's seminal paper [25], according to which a sufficient condition for the injectivity of a locally univalent meromorphic function can be given in terms of its Schwarzian derivative. In the setting of differential equations, Nehari's theorem [25, Theorem I] admits the following (equivalent) formulation: if A is analytic in $\mathbb{D}$ and

$$\sup_{z\in\mathbb{D}} |A(z)|(1-|z|^2)^2 \tag{1.1}$$

is at most one, then each non-trivial solution ($f \not\equiv 0$) of

$$f'' + Af = 0 \tag{1.2}$$

has at most one zero in $\mathbb{D}$. A few years later, in 1955, Schwarz showed [36, Theorems 3–4] that if A is analytic in $\mathbb{D}$ then zero-sequences of all non-trivial solutions of (1.2) are separated in the hyperbolic metric if and only if (1.1) is finite. The necessary condition, corresponding to Nehari's theorem, was given by Kraus [22]. For recent developments based on localization of the classical results, see [5]. In the case of higher order linear differential equations

$$f^{(k)} + A_{k-1}f^{(k-1)} + \cdots + A_1 f' + A_0 f = 0, \quad k \in \mathbb{N}, \tag{1.3}$$

Date: March 17, 2017.

2010 *Mathematics Subject Classification.* Primary 30H10, 34M10.

Key words and phrases. Growth of solution, Hardy space, linear differential equation.

The first author is supported in part by the Academy of Finland #286877; the second author is supported in part by the Academy of Finland #268009, and the Faculty of Science and Forestry of the University of Eastern Finland #930349; and the third author is supported in part by the Academy of Finland #268009, the Faculty of Science and Forestry of University of Eastern Finland #930349, La Junta de Andalucía (FQM210) and (P09-FQM-4468), and the grants MTM2011-25502, MTM2011-26538 and MTM2014-52865-P.

with analytic coefficients $A_0, \dots, A_{k-1}$, this line of reasoning has not given complete results. Some progress on the subject was obtained in the seventies and eighties by Kim and Lavie, among many other authors.

Nevanlinna and Wiman-Valiron theories, in the form they are known today, do not seem to be sufficiently delicate tools to study slowly growing solutions of (1.2), and hence different approach must be employed. An important breakthrough in this regard was [33], where Pommerenke obtained a sharp sufficient condition for the analytic coefficient A which places all solutions f of (1.2) to the classical Hardy space H^2. Pommerenke's idea was to use Green's formula twice to write the H^2-norm of f in terms of f'', employ the differential equation (1.2), and then apply Carleson's theorem for the Hardy spaces [8, Theorem 9.3]. Consequently, the coefficient condition was given in terms of Carleson measures. The leading idea of this (operator theoretic) approach has been extended to study, for example, solutions in the Hardy and Bergman spaces [28, 35], Dirichlet type spaces [19] and growth spaces [16, 21], to name a few instances.

Our intention is to establish sufficient conditions for the coefficient of (1.2) which place all solutions to H^∞, BMOA or to the Bloch space. In principle, Pommerenke's original idea could be modified to cover these cases, but in practice, this approach falls short since either it is difficult to find a useful expression for the norm in terms of the second derivative (in the case of H^∞) or the characterization of Carleson measures is not known (in the cases of BMOA and Bloch). Concerning Carleson measures for the Bloch space, see [13]. Curiously enough, the best known coefficient condition placing all solutions of (1.2) to the Bloch space is obtained by straightforward integration [21]. Our approach takes advantage of the reproducing formulae, and is different to ones in the literature.

2. Main results

Let $\mathcal{H}(\mathbb{D})$ denote the collection of functions analytic in $\mathbb{D}$, and let m be the Lebesgue area measure, normalized so that $m(\mathbb{D}) = 1$. By postponing the rigorous definitions to the forthcoming sections, we proceed to outline our results. We begin with the zero distribution of non-trivial solutions of the linear differential equation

$$f''' + A_2 f'' + A_1 f' + A_0 f = 0 \tag{2.1}$$

with analytic coefficients. Note that zeros of non-trivial solutions of (2.1) are at most two-fold. Let $\varphi_a(z) = (a - z)/(1 - \overline{a}z)$, for $a, z \in \mathbb{D}$, denote a conformal automorphism of $\mathbb{D}$ which coincides with its own inverse.

Theorem 1. *Let f be a non-trivial solution of (2.1) where $A_0, A_1, A_2 \in \mathcal{H}(\mathbb{D})$.*

(i) *If*

$$\sup_{z\in\mathbb{D}} |A_j(z)|(1 - |z|^2)^{3-j} < \infty, \quad j = 0, 1, 2, \tag{2.2}$$

then the sequence of two-fold zeros of f is a finite union of separated sequences.

(ii) *If*

$$\sup_{a\in\mathbb{D}} \int_{\mathbb{D}} |A_j(z)|(1 - |z|^2)^{1-j}\big(1 - |\varphi_a(z)|^2\big)\, dm(z) < \infty, \quad j = 0, 1, 2, \tag{2.3}$$

then the sequence of two-fold zeros of f is a finite union of uniformly separated sequences.

Theorem 1(i) should be compared to the second order case [36, Theorem 3], which was already mentioned in the introduction. For the second order counterpart of Theorem 1(ii), see [14, Theorem 1]. By a standard transformation as in [23, p. 74], both [36, Theorem 3] and [14, Theorem 1] admit immediate generalizations to second order differential equations (1.3) with an intermediate coefficient A_1. The proof of Theorem 1 is presented in Section 3, and it is based on a conformal transformation of (2.1), Jensen's formula, and on a sharp growth estimate for solutions of (2.1). Theorem 1 extends to

the case of higher order differential equations (1.3), but we leave details for the interested reader.

The following results concern slowly growing solutions of the second order differential equation (1.2), however, our methods could also be applied in more general situations. A sufficient condition for the analytic coefficient A, which forces all solutions of (1.2) to be bounded, is given in terms of Cauchy transforms. The space $\mathcal{K}$ of Cauchy transforms consists of functions in $\mathcal{H}(\mathbb{D})$ that take the form $\int_{\mathbb{T}}(1-\overline{\zeta}z)^{-1}\,d\mu(\zeta)$, where μ is a finite, complex, Borel measure on the unit circle $\mathbb{T}=\partial\mathbb{D}$. For more details we refer to Section 5, where the following theorem is proved.

Theorem 2. *Let $A\in\mathcal{H}(\mathbb{D})$.*

(i) *If $\limsup_{r\to 1^-}\sup_{z\in\mathbb{D}}\|A_{r,z}\|_{\mathcal{K}}<1$ for*

$$A_{r,z}(u)=\overline{\int_0^z\int_0^\zeta \frac{A(rw)}{1-\overline{u}w}\,dw\,d\zeta},\quad u\in\mathbb{D},$$

then all solutions of (1.2) *are bounded.*

(ii) *If a primitive of A belongs to the Hardy space H^1, then all solutions of* (1.2) *have their first derivative in H^1.*

For $f\in\mathcal{H}(\mathbb{D})$, $f'\in H^1$ if and only if f admits a continuous extension to $\overline{\mathbb{D}}$ and is absolutely continuous on $\mathbb{T}$ [8, Theorem 3.11]. Therefore, as a consequence of Theorem 2(ii), we obtain a coefficient condition which places all solutions of (1.2) to the disc algebra.

The question converse to Theorem 2(i) is open and appears to be difficult. The boundedness of one non-trivial solution of (1.2) is not enough to guarantee that (1.1) is finite, which can be easily seen by considering the solution $f(z)=\exp(-(1+z)/(1-z))$ of (1.2) for $A(z)=-4z/(1-z)^4$, $z\in\mathbb{D}$. However, if (1.2) admits linearly independent solutions $f_1,f_2\in H^\infty$ such that $\inf_{z\in\mathbb{D}}\big(|f_1(z)|+|f_2(z)|\big)>0$, then (1.1) is finite. This is a consequence of the Corona theorem [8, Theorem 12.1], according to which there exist $g_1,g_2\in H^\infty$ such that $f_1g_1+f_2g_2\equiv 1$, and consequently $A=A+(f_1g_1+f_2g_2)''=2(f_1'g_1'+f_2'g_2')+f_1g_1''+f_2g_2''$.

We proceed to consider BMOA, which consists of those functions in the Hardy space H^2 whose boundary values are of bounded mean oscillation. The following result should be compared to [33, Theorem 2] as BMOA is a conformally invariant subspace of H^2.

Theorem 3. *Let $A\in\mathcal{H}(\mathbb{D})$. If*

$$\sup_{a\in\mathbb{D}}\left(\log\frac{e}{1-|a|}\right)^2\int_{\mathbb{D}}|A(z)|^2(1-|z|^2)^2(1-|\varphi_a(z)|^2)\,dm(z) \tag{2.4}$$

is sufficiently small, then all solutions of (1.2) *belong to* BMOA.

To the best of our knowledge BMOA solutions of (1.2) have not been discussed in the literature before. The coefficient condition in Theorem 3 allows solutions of (1.2) to be unbounded, see Example 2 in Section 6. By [28, Lemma 5.3] or [40, Theorem 1], (2.4) is comparable to

$$\sup_{a\in\mathbb{D}}\frac{\big(\log\frac{e}{1-|a|}\big)^2}{1-|a|}\int_{S_a}|A(z)|^2(1-|z|^2)^3\,dm(z), \tag{2.5}$$

where $S_a=\{re^{i\theta}:|a|<r<1,\,|\theta-\arg(a)|\le(1-|a|)/2\}$ denotes the Carleson square with respect to $a\in\mathbb{D}\setminus\{0\}$ and $S_0=\mathbb{D}$. See also [37, Lemma 3.4]. Solutions in VMOA, the closure of polynomials in BMOA, are discussed in Section 6 in which Theorem 3 is proved.

The case of the Bloch space $\mathcal{B}$ is especially interesting. For $0<\alpha<\infty$, let $\mathcal{L}^\alpha$ denote the collection of those $A\in\mathcal{H}(\mathbb{D})$ for which

$$\|A\|_{\mathcal{L}^\alpha}=\sup_{z\in\mathbb{D}}|A(z)|(1-|z|^2)^2\left(\log\frac{e}{1-|z|}\right)^\alpha<\infty.$$

The comparison between H^∞_2, $\mathcal{L}^\alpha$ and the functions for which (2.4) is finite is presented in Section 4. It is known that, if $\|A\|_{\mathcal{L}^1}$ is sufficiently small, then all solutions of (1.2) belong to $\mathcal{B}$. This result was recently discovered with the best possible upper bound for $\|A\|_{\mathcal{L}^1}$ in [21, Corollary 4(b) and Example 5(b)]. Moreover, if $A \in \mathcal{L}^1$ then all solutions of (1.2) are in H^2 by [33, Corollary 1]. We point out that, if $A \in \mathcal{L}^\alpha$ for any $1 < \alpha < \infty$, then all solutions of (1.2) are bounded by [18, Theorem G(a)]. Solutions in the little Bloch space $\mathcal{B}_0$, the closure of polynomials in $\mathcal{B}$, are discussed in Section 7, among other results involving the Bloch space.

The proof of Theorem 2(i) is based on an application of the reproducing formula for H^1 functions, and it is natural to ask whether this method extends to the cases of $\mathcal{B}$ and BMOA. In the case of $\mathcal{B}$, by using the reproducing formula for weighted Bergman spaces, we prove a result (namely, Theorem 10) offering a family of coefficient conditions, which are given in terms of Bergman spaces induced by doubling weights. The case of BMOA, with the reproducing formula for H^1, is further considered in Section 8.

A careful reader observes that the results above are closely related to operator theory. If f is a solution of (1.2), then

$$f(z) = -\int_0^z \left(\int_0^\zeta f(w)A(w)\,dw \right) d\zeta + f'(0)z + f(0), \quad z \in \mathbb{D}. \tag{2.6}$$

By denoting

$$S_A(f)(z) = \int_0^z \left(\int_0^\zeta f(w)A(w)\,dw \right) d\zeta, \quad z \in \mathbb{D},$$

we obtain an integral operator, induced by the symbol $A \in \mathcal{H}(\mathbb{D})$, that sends $\mathcal{H}(\mathbb{D})$ into itself. With this approach, the search of sufficient coefficient conditions boils down to finding sufficient conditions for the boundedness of S_A. Therefore, it is not a surprise that many results on slowly growing solutions are inspired by study of the classical integral operator

$$T_g(f)(z) = \int_0^z f(\zeta)g'(\zeta)\,d\zeta,$$

see [2, 3, 7, 32, 38]. The strength of the operator theoretic approach is demonstrated by proving that the coefficient conditions arising from Theorem 10 are essentially interchangeable with $A \in \mathcal{L}^1$, see Theorem 11.

Deep duality relations are implicit in the proofs of Theorems 2(i), 10 and 14. The dual of H^1 is isomorphic to BMOA with the Cauchy pairing by Fefferman's theorem [12, Theorem 7.1], the dual of the disc algebra is isomorphic to the space of Cauchy transforms with the dual pairing $\langle f, K\mu\rangle = \int f\,\overline{d\mu}$ [6, Theorem 4.2.2], and the dual of A^1_ω is isomorphic to the Bloch space with the dual pairing $\langle f, g\rangle_{A^2_\omega} = \int_{\mathbb{D}} f\overline{g}\,\omega\,dm$ [30, Corollary 7].

Finally, we turn to consider coefficient conditions which place solutions of (1.2) in the Hardy spaces. Our results are inspired by an open question, which is closely related to the Hardy-Stein-Spencer formula

$$\|f\|^p_{H^p} = |f(0)|^p + \frac{p^2}{2}\int_{\mathbb{D}} |f(z)|^{p-2}|f'(z)|^2 \log\frac{1}{|z|}\,dm(z), \tag{2.7}$$

that holds for $0 < p < \infty$ and $f \in \mathcal{H}(\mathbb{D})$. For $p = 2$, (2.7) is the well-known Littlewood-Paley identity, while the general case follows from [17, Theorem 3.1] by integration.

Question 1. Let $0 < p < \infty$. Is it true that

$$\|f\|^p_{H^p} \leq C(p)\int_{\mathbb{D}} |f(z)|^{p-2}|f''(z)|^2(1-|z|^2)^3\,dm(z) + |f(0)|^p + |f'(0)|^p \tag{2.8}$$

for any $f \in \mathcal{H}(\mathbb{D})$, where $C(p)$ is a positive constant such that $C(p) \to 0^+$ as $p \to 0^+$?

Affirmative answer to this question would have an immediate application to differential equations, see Section 9.2. In the context of second order differential equation (1.2), it suffices to consider Question 1 under the additional assumptions that all zeros of f are simple and f'' vanishes at zeros of f. The estimate in Question 1 is valid for a non-trivial subclass of $\mathcal{H}(\mathbb{D})$, see Section 9.1.

Function $f \in \mathcal{H}(\mathbb{D})$ is uniformly locally univalent if there is a constant $0 < \delta \leq 1$ such that f is univalent in each pseudo-hyperbolic disc $\Delta(z, \delta) = \{w \in \mathbb{D} : |\varphi_z(w)| < \delta\}$ for $z \in \mathbb{D}$. A partial solution to Question 1 is given by Theorem 4. Here $a \lesssim b$ means that there exists $C > 0$ such that $a \leq Cb$. Moreover, $a \asymp b$ if and only if $a \lesssim b$ and $a \gtrsim b$.

Theorem 4. *Let $f \in \mathcal{H}(\mathbb{D})$, and $k \in \mathbb{N}$.*

(i) *If $0 < p \leq 2$, then*

$$\|f\|_{H^p}^p \lesssim \int_{\mathbb{D}} |f(z)|^{p-2} |f^{(k)}(z)|^2 (1 - |z|^2)^{2k-1} \, dm(z) + \sum_{j=0}^{k-1} |f^{(j)}(0)|^p. \tag{2.9}$$

(ii) *If $2 \leq p < \infty$, then*

$$\int_{\mathbb{D}} |f(z)|^{p-2} |f^{(k)}(z)|^2 (1 - |z|^2)^{2k-1} \, dm(z) + \sum_{j=0}^{k-1} |f^{(j)}(0)|^p \lesssim \|f\|_{H^p}^p. \tag{2.10}$$

(iii) *If $0 < p < \infty$ and f is uniformly locally univalent, then* (2.10) *holds.*

The comparison constants are independent of f; in (i) *and* (ii) *they depend on p, and in* (iii) *it depends on δ (the constant of uniform local univalence) and p.*

The proof of Theorem 4 is presented in Section 9, and it takes advantage of a norm in H^p, given in terms of higher derivatives and area functions, and an estimate of the non-tangential maximal function.

3. Zero distribution of solutions

For $0 \leq p < \infty$, the growth space H_p^∞ consists of those $g \in \mathcal{H}(\mathbb{D})$ for which

$$\|g\|_{H_p^\infty} = \sup_{z \in \mathbb{D}} |g(z)|(1 - |z|^2)^p < \infty.$$

We write $H^\infty = H_0^\infty$, for short. The sequence $\{z_n\}_{n=1}^\infty \subset \mathbb{D}$ is called uniformly separated if

$$\inf_{k \in \mathbb{N}} \prod_{n \in \mathbb{N} \setminus \{k\}} \left| \frac{z_n - z_k}{1 - \overline{z}_n z_k} \right| > 0,$$

while $\{z_n\}_{n=1}^\infty \subset \mathbb{D}$ is said to be separated in the hyperbolic metric if there exists a constant $\delta > 0$ such that $|z_n - z_k|/|1 - \overline{z}_n z_k| > \delta$ for any $n \neq k$. After the proof of Theorem 1, we present an auxiliary result which provides an estimate for the number of sequences in the finite union appearing in the claim.

Proof of Theorem 1. (i) If f is a non-trivial solution of (2.1), then $g = f \circ \varphi_a$ solves

$$g''' + B_2 g'' + B_1 g' + B_0 g = 0, \tag{3.1}$$

where

$$\begin{aligned} B_0 &= (A_0 \circ \varphi_a)(\varphi_a')^3, \qquad B_2 = (A_2 \circ \varphi_a)\varphi_a' - 3\,\frac{\varphi_a''}{\varphi_a'}, \\ B_1 &= (A_1 \circ \varphi_a)(\varphi_a')^2 - (A_2 \circ \varphi_a)\varphi_a'' + 3\left(\frac{\varphi_a''}{\varphi_a'}\right)^2 - \frac{\varphi_a'''}{\varphi_a'}. \end{aligned} \tag{3.2}$$

By a conformal change of variable, we deduce $\|B_0\|_{H^\infty_3} = \|A_0\|_{H^\infty_3}$,

$$\begin{aligned}\|B_2\|_{H^\infty_1} &\leq \sup_{z\in\mathbb{D}} |A_2(z)|\,(1-|z|^2) + \sup_{z\in\mathbb{D}} \frac{6|a|}{|1-\overline{a}z|}\,(1-|z|^2) \leq \|A_2\|_{H^\infty_1} + 12,\\ \|B_1\|_{H^\infty_2} &\leq \sup_{z\in\mathbb{D}} |A_1(z)|\,(1-|z|^2)^2 + \sup_{w\in\mathbb{D}} |A_2(w)|\,(1-|w|^2)\left|\frac{\varphi_a''(\varphi_a(w))}{\varphi_a'(\varphi_a(w))}\right|(1-|\varphi_a(w)|^2)\\ &\quad + \sup_{z\in\mathbb{D}} \frac{12|a|^2}{|1-\overline{a}z|^2}\,(1-|z|^2)^2 + \sup_{z\in\mathbb{D}} \frac{6|a|^2}{|1-\overline{a}z|^2}\,(1-|z|^2)^2\\ &\leq \|A_1\|_{H^\infty_2} + 4\|A_2\|_{H^\infty_1} + 72.\end{aligned}$$

Let $\mathcal{Z} = \mathcal{Z}(f)$ be the sequence of two-fold zeros of f, and let $a \in \mathcal{Z}$; we may assume that $\mathcal{Z}$ is not empty, for otherwise there is nothing to prove. Then, the zero of $g = f \circ \varphi_a$ at the origin is two-fold. By applying Jensen's formula to $z \mapsto g(z)/z^2$ we obtain

$$\sum_{\substack{z_k\in\mathcal{Z}\\ 0<|\varphi_a(z_k)|<r}} \log\frac{r}{|\varphi_a(z_k)|} \leq \frac{1}{2\pi}\int_0^{2\pi} \log^+\left|\frac{g(re^{i\theta})}{g''(0)}\right| d\theta + \log\frac{2}{r^2}, \quad 0<r<1, \tag{3.3}$$

where $\log^+ x = \max\{0, \log x\}$ for $0 \leq x < \infty$. Since

$$\begin{aligned}\int_0^1 \left(\sum_{\substack{z_k\in\mathcal{Z}\\ 0<|\varphi_a(z_k)|<r}} \log\frac{r}{|\varphi_a(z_k)|}\right) r\,dr &= \sum_{z_k\in\mathcal{Z}\setminus\{a\}} \int_{|\varphi_a(z_k)|}^1 r\log\frac{r}{|\varphi_a(z_k)|}\,dr\\ &\geq \frac{1}{8}\sum_{z_k\in\mathcal{Z}\setminus\{a\}} \big(1-|\varphi_a(z_k)|^2\big)^2,\end{aligned}$$

the estimate (3.3) implies

$$\sum_{z_k\in\mathcal{Z}\setminus\{a\}} \big(1-|\varphi_a(z_k)|^2\big)^2 \leq 4\int_{\mathbb{D}} \log^+\left|\frac{g(z)}{g''(0)}\right| dm(z) + 4\log 2 + 4.$$

Consider the normalized solution $h(z) = g(z)/g''(0)$ of (3.1), which has the initial values $h(0) = h'(0) = 0$ and $h''(0) = 1$. By the proofs of the growth estimates [18, Theorems 3.1 and 4.1, and Corollary 4.2], there exists an absolute constant $C_1 > 0$ such that

$$\frac{1}{2\pi}\int_0^{2\pi} \log^+\big|h(re^{i\theta})\big|\,d\theta \leq C_1 \sum_{j=0}^{2}\sum_{n=0}^{j}\int_0^{2\pi}\int_0^r |B_j^{(n)}(se^{i\theta})|(1-s)^{3-j+n-1}\,ds\,d\theta.$$

By Cauchy's integral formula and the estimates above, there exists a positive constant $C_2 = C_2(\|A_0\|_{H^\infty_3}, \|A_1\|_{H^\infty_2}, \|A_2\|_{H^\infty_1})$, independent of $a \in \mathbb{D}$, such that

$$\big\|B_j^{(n)}\big\|_{H^\infty_{3-j+n}} \leq C_2, \quad j = 0,1,2, \quad n = 0,\ldots,j.$$

Let $M_\infty\big(s, B_j^{(n)}\big)$ denote the maximum modulus of $B_j^{(n)}$ on the circle of radius s. Now

$$\begin{aligned}&\sup_{a\in\mathcal{Z}} \sum_{z_k\in\mathcal{Z}\setminus\{a\}} \big(1-|\varphi_a(z_k)|^2\big)^2\\ &\quad\leq 4\log 2 + 4 + 16\pi\,C_1 \sup_{a\in\mathcal{Z}} \sum_{j=0}^{2}\sum_{n=0}^{j}\int_0^1\int_0^r M_\infty\big(s, B_j^{(n)}\big)(1-s)^{2-j+n}\,ds\,dr\\ &\quad\leq 4\log 2 + 4 + 16\pi\,C_1C_2 \sum_{j=0}^{2}\sum_{n=0}^{j}\int_0^1\int_0^r \frac{ds}{1-s^2}\,dr < \infty.\end{aligned}$$

The assertion of Theorem 1(i) follows from Lemma 5(i) below.

(ii) As in the proof of (i), we conclude that $g = f \circ \varphi_a$ is a solution of (3.1), where the coefficients B_0, B_1, B_2 depend on $a \in \mathbb{D}$. By (2.3),

$$\sup_{a\in\mathbb{D}} \int_{\mathbb{D}} |B_j^{(n)}(z)|(1-|z|^2)^{2-j+n}\, dm(z) < \infty, \quad j = 0, \dots, 2, \quad n = 0, \dots, j. \tag{3.4}$$

In order to conclude (3.4), first get rid of the derivatives by standard estimates, and then integrate the coefficients (3.2) term-by-term.

Let $\mathcal{Z}$ be the sequence of two-fold zeros of f. As above, there exists an absolute constant $C_3 > 0$ such that

$$\sup_{a\in\mathcal{Z}} \sum_{\substack{z_k\in\mathcal{Z}\\ 0<|\varphi_a(z_k)|<r}} \log\frac{r}{|\varphi_a(z_k)|} \le \log\frac{2}{r^2} + C_3 \sup_{a\in\mathcal{Z}} \sum_{j=0}^{2}\sum_{n=0}^{j} \int_{\mathbb{D}} |B_j^{(n)}(z)|(1-|z|^2)^{2-j+n}\, dm(z)$$

for $0 < r < 1$. By letting $r \to 1^-$, we obtain

$$\sup_{a\in\mathcal{Z}} \sum_{z_k\in\mathcal{Z}\setminus\{a\}} \big(1-|\varphi_a(z_k)|^2\big) < \infty.$$

This implies the assertion of Theorem 1(ii) by Lemma 5(ii) below. □

The following lemma gives an estimate for the number of sequences in the finite union appearing in the statement of Theorem 1. For more details, we refer to [9, Chapter 2.11].

Lemma 5. *Let $\mathcal{Z} = \{z_k\}$ be a sequence of points in $\mathbb{D}$ such that the multiplicity of each point is at most $p \in \mathbb{N}$, and let $M \in \mathbb{N}$.*

(i) *If*

$$\sup_{a\in\mathcal{Z}} \sum_{z_k\in\mathcal{Z}\setminus\{a\}} \big(1-|\varphi_a(z_k)|^2\big)^2 \le M < \infty,$$

then $\{z_k\}$ can be expressed as a finite union of at most $M+p$ separated sequences.

(ii) *If*

$$\sup_{a\in\mathcal{Z}} \sum_{z_k\in\mathcal{Z}\setminus\{a\}} \big(1-|\varphi_a(z_k)|^2\big) \le M < \infty, \tag{3.5}$$

then $\{z_k\}$ can be expressed as a finite union of at most $M+p$ uniformly separated sequences.

Proof. (i) Assume on contrary to the claim, that every partition of $\mathcal{Z}$ into separated subsequences is a union of at least $M+p+1$ sequences. Then, for each $n \in \mathbb{N}$, there exists a point $z_n \in \mathcal{Z}$ such that

$$\#\big\{z_k \in \mathcal{Z} : |\varphi_{z_n}(z_k)| \le 2^{-n}\big\} \ge M+p+1.$$

Now

$$\begin{aligned} p+M &\ge p + \sum_{z_k\in\mathcal{Z}\setminus\{z_n\}} \big(1-|\varphi_{z_n}(z_k)|^2\big)^2 \ge \sum_{z_k\in\mathcal{Z}} \big(1-|\varphi_{z_n}(z_k)|^2\big)^2 \\ &\ge \#\big\{z_k \in \mathcal{Z} : |\varphi_{z_n}(z_k)| \le 2^{-n}\big\}\cdot(1-4^{-n})^2 \ge (M+p+1)(1-4^{-n})^2. \end{aligned}$$

By letting $n \to \infty$ we arrive to a contradiction. Hence $\mathcal{Z}$ can be expressed as a union of at most $M+p$ separated sequences.

(ii) By part (i), $\mathcal{Z}$ can be expressed as a union of at most $M+p$ separated sequences, and each of these separated sequences is uniformly separated by (3.5). □

Example 1. If $\{f, g\}$ is a solution base of (1.2), then $\{f^2, g^2, fg\}$ is a solution base of

$$h''' + 4Ah' + 2A'h = 0. \tag{3.6}$$

Let us apply this property to a classical example [36, p. 162] originally due to Hille [20, p. 552]. For $\gamma > 0$, the differential equation (1.2) with $A(z) = (1+4\gamma^2)/(1-z^2)^2$, $z \in \mathbb{D}$, admits the solution

$$f(z) = \sqrt{1-z^2}\,\sin\left(\gamma \log \frac{1+z}{1-z}\right), \quad z \in \mathbb{D}.$$

The zeros of f are simple and real, and moreover, the hyperbolic distance between two consecutive zeros is precisely $\pi/(2\gamma)$. Consequently, (3.6) admits the solution $h = f^2$ whose zero-sequence is a union of two separated sequences. This sequence is a union of two uniformly separated sequences (in fact, a union of two exponential sequences), since all zeros are real [8, Theorem 9.2]. In this case the coefficients of (3.6) satisfy both conditions (2.2) and (2.3). ◇

4. Inclusion relations between function spaces

The following result can be used to compare the coefficient conditions. In particular, Lemma 6 shows that the coefficient condition in Theorem 3 (which implies that all solutions of (1.2) are in BMOA) is strictly stronger than $A \in \mathcal{L}^1$ with sufficiently small norm (which places all solutions in $\mathcal{B} \cap H^2$). And further, Lemma 6 proves that $A \in \mathcal{L}^1$ with sufficiently small norm is strictly stronger than the coefficient condition in Theorem A below (which forces solutions to be in Hardy spaces). The reader is invited to compare Lemma 6 to the results in [4, Section 5].

If $A \in \mathcal{H}(\mathbb{D})$ and

$$\sup_{a\in\mathbb{D}} \int_{\mathbb{D}} |A(z)|^2(1-|z|^2)^2(1-|\varphi_a(z)|^2)\,dm(z) \tag{4.1}$$

is finite, then we write $A \in \mathrm{BMOA}''$. Note that $A \in \mathrm{BMOA}''$ if and only if there exists a function $g = g(A) \in \mathrm{BMOA}$ such that $A = g''$, which follows from standard estimates. Correspondingly, if $A \in \mathcal{H}(\mathbb{D})$ and

$$\|A\|^2_{\mathrm{LMOA}''} = \sup_{a\in\mathbb{D}} \left(\log \frac{e}{1-|a|}\right)^2 \int_{\mathbb{D}} |A(z)|^2(1-|z|^2)^2(1-|\varphi_a(z)|^2)\,dm(z) < \infty,$$

then $A \in \mathrm{LMOA}''$. As expected, LMOA'' consists of those functions in $\mathcal{H}(\mathbb{D})$ which can be represented as the second derivative of a function in LMOA. For more details on LMOA, see [4, 37]. Finally, part (iv) of Lemma 6 gives a sufficient condition for a lacunary series to be in LMOA''.

Lemma 6. *The following assertions hold:*

(i) $\mathcal{L}^{\alpha_1} \subsetneq \mathcal{L}^{\alpha_2} \subsetneq H^\infty_2$ *for any* $0 < \alpha_2 < \alpha_1 < \infty$;
(ii) $\mathrm{LMOA}'' \subsetneq \mathcal{L}^1 \subsetneq \mathcal{L}^\alpha \subsetneq \mathrm{BMOA}'' \subsetneq H^\infty_2$ *for any* $1/2 < \alpha < 1$;
(iii) $\mathcal{L}^{3/2} \subsetneq \mathrm{LMOA}''$, *and* $\mathrm{LMOA}'' \setminus \bigcup_{1<\alpha<\infty} \mathcal{L}^\alpha$ *is non-empty;*
(iv) *if* $\{n_k\}_{k=1}^\infty \subset \mathbb{N}$ *and* $\{a_k\}_{k=1}^\infty \subset \mathbb{C}$ *satisfy the conditions* $\inf_{k\in\mathbb{N}} n_{k+1}/n_k > 1$ *and* $\sum_{k=1}^\infty |a_k|^2(\log n_k)^3/n_k^4 < \infty$, *then* $\left(\sum_{k=1}^\infty a_k z^{n_k}\right) \in \mathrm{LMOA}''$.

Proof. As (i) is an immediate consequence of the definitions, we proceed to prove (ii). Let $A \in \mathrm{LMOA}''$. Since (2.5) is finite and $|A|^2$ is subharmonic, we deduce $\|A\|^2_{\mathcal{L}^1} \lesssim \|A\|^2_{\mathrm{LMOA}''}$. Assume on contrary to the assertion that $\mathrm{LMOA}'' = \mathcal{L}^1$. By [15, Theorem 1], there exist $A_0, A_1 \in \mathcal{H}(\mathbb{D})$ satisfying

$$|A_0(z)| + |A_1(z)| \asymp \frac{1}{(1-|z|^2)^2 \log\frac{e}{1-|z|}}, \quad z \in \mathbb{D}.$$

Since $A_0, A_1 \in \mathrm{LMOA}''$, we deduce

$$\int_{S_a} \frac{dm(z)}{(1-|z|^2)\big(\log\frac{e}{1-|z|}\big)^2} \lesssim \int_{S_a} \big(|A_0(z)| + |A_1(z)|\big)^2(1-|z|^2)^3\,dm(z) \lesssim \frac{1-|a|}{\big(\log\frac{e}{1-|a|}\big)^2}$$

as $|a| \to 1^-$. This contradicts the fact

$$\int_{S_a} \frac{dm(z)}{(1-|z|^2)\big(\log \frac{e}{1-|z|}\big)^2} \asymp \frac{1-|a|}{\log \frac{e}{1-|a|}}, \quad |a| \to 1^-,$$

and hence $\mathrm{LMOA}'' \neq \mathcal{L}^1$. The remaining part of (ii) is a straightforward computation. Note that the inclusion $\mathcal{L}^\alpha \subsetneq \mathrm{BMOA}''$, for any $1/2 < \alpha < \infty$, is strict by $A(z) = (1-z)^{-2}$.

To prove (iii) it suffices to prove the latter assertion, as $\mathcal{L}^{3/2} \subset \mathrm{LMOA}''$ follows directly from (2.5). If $A(z) = (1-z)^{-2}\big(\log \frac{e}{1-z}\big)^{-1}$ for $z \in \mathbb{D}$, then $A \notin \bigcup_{1<\alpha<\infty} \mathcal{L}^\alpha$. To show that $A \in \mathrm{LMOA}''$, it is enough to verify (2.5) for $0 < a < 1$. Since

$$\left|\log \frac{e}{1-z}\right| \geq \log \frac{e}{|1-z|} \geq \log \frac{e}{2(1-a)}, \quad z \in S_a, \tag{4.2}$$

we conclude

$$\begin{aligned} &\sup_{0<a<1} \frac{\Big(\log \frac{e}{1-a}\Big)^2}{1-a} \int_{S_a} |A(z)|^2 (1-|z|^2)^3 \, dm(z) \\ &\qquad \lesssim \sup_{0<a<1} \frac{1}{1-a} \int_a^1 \int_0^{2\pi} \frac{d\theta}{|1-re^{i\theta}|^4} (1-r^2)^3 \, r \, dr < \infty. \end{aligned} \tag{4.3}$$

In order to prove (iv), let $A(z) = \sum_{k=1}^\infty a_k z^{n_k}$ for $z \in \mathbb{D}$. If $h(z) = \sum_{k=1}^\infty z^{n_k}$ for $z \in \mathbb{D}$, then $h \in \mathcal{B}$ with $M_\infty(r,h) = \sum_{k=1}^\infty r^{n_k} \lesssim \log \frac{e}{1-r}$ for $0 < r < 1$. By the Cauchy-Schwarz inequality,

$$M_\infty(r,A) \lesssim \left(\sum_{k=1}^\infty |a_k|^2 r^{n_k}\right)^{1/2} \left(\log \frac{e}{1-r}\right)^{1/2}, \quad 0 < r < 1.$$

It follows that

$$\begin{aligned} &\sup_{a\in\mathbb{D}} \frac{\big(\log \frac{e}{1-|a|}\big)^2}{1-|a|} \int_{S_a} |A(z)|^2 (1-|z|^2)^3 \, dm(z) \\ &\quad \lesssim \int_0^1 M_\infty(r,A)^2 (1-r)^3 \left(\log \frac{e}{1-r}\right)^2 dr \\ &\quad \lesssim \sum_{k=1}^\infty |a_k|^2 \int_0^1 r^{n_k} (1-r)^3 \left(\log \frac{e}{1-r}\right)^3 dr \asymp \sum_{k=1}^\infty |a_k|^2 \, \frac{(\log n_k)^3}{n_k^4}, \end{aligned}$$

where the asymptotic equality follows from [28, Lemma 1.3]. This completes the proof of Lemma 6. □

5. Bounded solutions

We consider bounded solutions of (1.2). As usual, the space H^∞ consists of $f \in \mathcal{H}(\mathbb{D})$ for which $\|f\|_{H^\infty} = \sup_{z\in\mathbb{D}} |f(z)| < \infty$. The proof of Theorem 2(i) takes advantage of the well-known representation formula

$$g(\zeta) = \frac{1}{2\pi} \int_0^{2\pi} \frac{g(e^{it})}{1-e^{-it}\zeta} \, dt, \quad \zeta \in \mathbb{D}, \tag{5.1}$$

which holds for any $g \in H^1$ [8, Theorem 3.6].

Let M be the collection of all (finite) complex Borel measures on $\mathbb{T}$. For $\mu \in M$, the total variation measure $|\mu|$ is defined as a set function

$$|\mu|(E) = \sup \sum_j |\mu(E_j)|,$$

where the supremum is taken over all countable (Borel) partitions $\{E_j\}$ of $E \subset \mathbb{T}$. Moreover, $\|\mu\| = |\mu|(\mathbb{T})$ is the total variation of μ [34, Chapter 6]. Let $\mathcal{K}$ be the space of Cauchy transforms, which consists of analytic functions in $\mathbb{D}$ of the form

$$(K\mu)(z) = \int_{\mathbb{T}} \frac{d\mu(\zeta)}{1-\overline{\zeta}z}, \quad z \in \mathbb{D},$$

for some $\mu \in M$. For each $f \in \mathcal{K}$ there is a set $M_f = \big\{\mu \in M : f = K\mu\big\}$ of measures that represent f, and produce the norm

$$\|f\|_{\mathcal{K}} = \inf\big\{\|\mu\| : \mu \in M_f\big\}.$$

We refer to [6] for more details.

Proof of Theorem 2(i). Let f be any solution of (1.2), and write $f_r(z) = f(rz)$ for $0 \leq r < 1$. Then f_r is analytic in $\overline{\mathbb{D}}$ and satisfies $f_r''(w) + r^2 A(rw) f_r(w) = 0$ for $w \in \mathbb{D}$. By (2.6), (5.1) for $g = f_r$, and Fubini's theorem, we conclude

$$f_r(z) = -\frac{1}{2\pi}\int_0^{2\pi} f_r(e^{it}) \int_0^z \int_0^\zeta \frac{r^2 A(rw)}{1-e^{-it}w}\, dw\, d\zeta\, dt + f_r'(0)z + f_r(0), \quad z \in \mathbb{D}.$$

For all $0 < r < 1$ sufficiently large, and $z \in \mathbb{D}$, there exists $\mu_{r,z} \in M$ such that

$$A_{r,z}(u) = (K\mu_{r,z})(u), \quad u \in \mathbb{D}, \tag{5.2}$$

and $\|\mu_{r,z}\| < \delta$ for some absolute constant $0 < \delta < 1$. Hence, by [6, Theorem 4.2.2],

$$\begin{aligned} f_r(z) &= -\frac{r^2}{2\pi}\int_0^{2\pi} f_r(e^{it})\overline{(K\mu_{r,z})(e^{it})}\, dt + f_r'(0)z + f_r(0) \\ &= -r^2 \int_{\mathbb{T}} f_r(x)\overline{d\mu_{r,z}(x)} + f_r'(0)z + f_r(0), \quad z \in \mathbb{D}. \end{aligned}$$

By [34, Theorem 6.12], there exist measurable functions $h_{r,z}$ such that $|h_{r,z}(\zeta)| = 1$ for all $\zeta \in \mathbb{T}$ and the polar decompositions $d\mu_{r,z} = h_{r,z}\, d|\mu_{r,z}|$ hold. Therefore

$$\begin{aligned} |f_r(z)| &\leq \left|\int_{\mathbb{T}} f_r(x)\overline{h_{r,z}(x)}\, d|\mu_{r,z}|(x)\right| + |f_r'(0)| + |f_r(0)| \\ &\leq \|f_r\|_{H^\infty}\int_{\mathbb{T}} d|\mu_{r,z}| + |f_r'(0)| + |f_r(0)| \\ &\leq \|f_r\|_{H^\infty}\|\mu_{r,z}\| + |f'(0)| + |f(0)|, \quad z \in \mathbb{D}. \end{aligned}$$

This implies $\|f\|_{H^\infty} \leq (|f(0)| + |f'(0)|)/(1-\delta)$, and hence completes the proof of Theorem 2(i). □

Let $0 < p < \infty$, $n \in \mathbb{N}$ and $f \in \mathcal{H}(\mathbb{D})$. The proof of Theorem 2(ii) relies on a classical representation

$$\|f\|_{H^p}^p \asymp \int_{\mathbb{T}} \left(\int_{\Gamma(\zeta)} |f^{(n)}(z)|^2 (1-|z|^2)^{2n-2}\, dm(z)\right)^{p/2} |d\zeta| + \sum_{j=0}^{n-1} |f^{(j)}(0)|^p, \tag{5.3}$$

which involves non-tangential approach regions; see [1, p. 125], for example. Hardy spaces H^p are further considered in Section 9. For a fixed $1 < \alpha < \infty$, the non-tangential approach region of aperture $2\arctan\sqrt{\alpha^2-1}$, with vertex at $\zeta \in \mathbb{T}$, is given by $\Gamma(\zeta) = \{z \in \mathbb{D} : |z-\zeta| \leq \alpha(1-|z|)\}$. The corresponding non-tangential maximal function is

$$f^\star(\zeta) = \sup_{z \in \Gamma(\zeta)} |f(z)|, \quad \zeta \in \mathbb{T}. \tag{5.4}$$

Proof of Theorem 2(ii). Let $A(z) = \sum_{n=0}^\infty a_n z^n$ for $z \in \mathbb{D}$. By the assumption, $\mathcal{A}(z) = \int_0^z A(\zeta)\, d\zeta$ satisfies $\mathcal{A} \in H^1$. We compute

$$\int_0^1 M_\infty(r, A)(1-r)\, dr \leq \int_0^1 \left(\sum_{n=0}^\infty |a_n| r^n\right)(1-r)\, dr = \sum_{n=0}^\infty \frac{|a_n|}{(n+1)(n+2)} \leq \pi\, \|\mathcal{A}\|_{H^1},$$

where the last estimate follows from Hardy's inequality [8, p. 48]. By [19, Corollary 3.16], we conclude that all solutions of (1.2) are bounded.

Let f be a solution of (1.2). Then

$$f'(z) = -\int_0^z f(\zeta)A(\zeta)\,d\zeta + f'(0), \quad z \in \mathbb{D},$$

and hence by (5.3), we deduce

$$\begin{aligned}\|f'\|_{H^1} &\leq \left\| \int_0^z f(\zeta)A(\zeta)\,d\zeta \right\|_{H^1} + |f'(0)| \\ &\asymp \int_{\mathbb{T}} \left(\int_{\Gamma(\zeta)} |f(z)|^2 |A(z)|^2\,dm(z) \right)^{1/2} |d\zeta| + |f'(0)| + |f''(0)| \\ &\leq \|f\|_{H^\infty} \|\mathcal{A}\|_{H^1} + |f'(0)| + |f''(0)|.\end{aligned}$$

The assertion $f' \in H^1$ follows. □

Remark 1. For each $0 < r < 1$ and $z \in \mathbb{D}$, it is easy to see that

$$d\widetilde{\mu}_{r,z}(x) = \overline{\left(\int_0^z \int_0^\zeta \frac{A(rw)}{x-w}\,dw\,d\zeta \right) \frac{dx}{2\pi i}}, \quad x \in \mathbb{T},$$

is one of the representing measures for which (5.2) holds, and hence $\|A_{r,z}\|_{\mathcal{K}} \leq \|\widetilde{\mu}_{r,z}\|$. Moreover, the behavior of the second primitive of A is controlled by this measure in the sense that

$$\int_0^z \int_0^\zeta A(rw)\,dwd\zeta = \int_0^z \int_0^\zeta \left(\frac{1}{2\pi i} \int_{\mathbb{T}} \frac{dx}{x-w} \right) A(rw)\,dwd\zeta = \int_{\mathbb{T}} \overline{d\widetilde{\mu}_{r,z}(x)},$$

which follows from Cauchy's integral formula and Fubini's theorem.

6. Solutions of bounded and vanishing mean oscillation

The space BMOA consists of those $f \in \mathcal{H}(\mathbb{D})$ for which

$$\|f\|^2_{\mathrm{BMOA}} = \sup_{a \in \mathbb{D}} \|f_a\|^2_{H^2} < \infty, \tag{6.1}$$

where $f_a(z) = f(\varphi_a(z)) - f(a)$ for $a, z \in \mathbb{D}$. By the Littlewood-Paley identity,

$$\|f\|^2_{\mathrm{BMOA}} \leq 4 \sup_{a \in \mathbb{D}} \int_{\mathbb{D}} |f'(z)|^2 (1 - |\varphi_a(z)|^2)\,dm(z) \leq 4\,\|f\|^2_{\mathrm{BMOA}}, \tag{6.2}$$

see [11, pp. 228–230]. Clearly, BMOA is a subspace of the Bloch space $\mathcal{B}$.

A positive Borel measure μ on $\mathbb{D}$ is called a Carleson measure, if

$$\|\mu\|_{\mathrm{Carleson}} = \sup_{a \in \mathbb{D}} \frac{\mu(S_a)}{1 - |a|} < \infty.$$

There exists a constant $1 \leq \alpha < \infty$ such that

$$\frac{1}{1-|a|} \leq \alpha\,\frac{1-|a|^2}{|1-\overline{a}z|^2} = \alpha\,|\varphi_a'(z)|, \quad z \in S_a, \quad a \in \mathbb{D},$$

since $|1 - \overline{a}z| \leq |1 - |a|^2| + ||a|^2 - \overline{a}z| \lesssim 1 - |a|$. Consequently,

$$\|\mu\|_{\mathrm{Carleson}} = \sup_{a \in \mathbb{D}} \int_{S_a} \frac{1}{1-|a|}\,d\mu(z) \leq \alpha \cdot \sup_{a \in \mathbb{D}} \int_{\mathbb{D}} |\varphi_a'(z)|\,d\mu(z). \tag{6.3}$$

We prove Theorem 3 and consider its counterpart for VMOA. Theorem 3 is inspired by [37, Theorem 3.1]. We return to consider BMOA and VMOA solutions in Section 8, where parallel results are obtained by using the representation formula for H^1 functions.

Proof of Theorem 3. The proof consists of two steps. First, we show that

$$\sup_{1/2<r<1}\sup_{a\in\mathbb{D}}\left(\log\frac{e}{1-|a|}\right)^2\int_{\mathbb{D}}|A(rz)|^2(1-|z|^2)^2(1-|\varphi_a(z)|^2)\,dm(z)\lesssim\|A\|^2_{\mathrm{LMOA}''}. \quad (6.4)$$

Denote

$$I(a,r)=\int_{\mathbb{D}}|A(rz)|^2(1-|z|^2)^2(1-|\varphi_a(z)|^2)\,dm(z),\quad 0<r<1,\quad a\in\mathbb{D},$$

for short. For $|a|\leq 1/2$ the estimate (6.4) is trivial. Let $1/2<|a|<1/(2-r)$. Since $|1-\overline{a}z|\leq 2\,|1-\overline{a}z/r|$ for $|z|\leq r$, we deduce

$$\begin{aligned}I(a,r)&=\int_{D(0,r)}|A(z)|^2\big(1-\big|\tfrac{z}{r}\big|^2\big)^3\frac{1-|a|^2}{\big|1-\overline{a}\,\frac{z}{r}\big|^2}\,\frac{dm(z)}{r^2}\\&\leq\frac{4}{r^2}\int_{\mathbb{D}}|A(z)|^2(1-|z|^2)^2(1-|\varphi_a(z)|^2)\,dm(z)\leq 16\,\|A\|^2_{\mathrm{LMOA}''}\left(\log\frac{e}{1-|a|}\right)^{-2}.\end{aligned}$$

for any $1/2<r<1$. Let $1/(2-r)\leq|a|<1$. Now

$$\begin{aligned}I(a,r)&\leq\|A\|^2_{\mathcal{L}^1}\int_{\mathbb{D}}\frac{\big(1-|z|^2\big)^2\big(1-|\varphi_a(z)|^2\big)}{\big(1-|rz|^2\big)^4\big(\log\frac{e}{1-|rz|}\big)^2}\,dm(z)\\&\lesssim\|A\|^2_{\mathcal{L}^1}\int_0^1\frac{(1-s)^3(1-|a|)}{(1-rs)^4\big(\log\frac{e}{1-rs}\big)^2(1-|a|s)}\,ds.\end{aligned}$$

As $t\mapsto(1-t)^2\big(\log\frac{e}{1-t}\big)$ is decreasing for $0<t<1$, we apply $r\leq 2-1/|a|$ to obtain

$$\begin{aligned}I(a,r)&\lesssim\|A\|^2_{\mathcal{L}^1}(1-|a|)\int_0^{|a|}\frac{ds}{(1-s)^2\big(\log\frac{e}{1-s}\big)^2}+\frac{\|A\|^2_{\mathcal{L}^1}}{(1-|a|)^4\big(\log\frac{e}{1-|a|}\big)^2}\int_{|a|}^1(1-s)^3\,ds\\&\lesssim\|A\|^2_{\mathcal{L}^1}\left(\log\frac{e}{1-|a|}\right)^{-2}.\end{aligned}$$

Since $\|A\|^2_{\mathcal{L}^1}\lesssim\|A\|^2_{\mathrm{LMOA}''}$ by the proof of Lemma 6(ii), this completes the proof of (6.4).

Second, we proceed to consider the differential equation (1.2). Let f be a non-trivial solution of (1.2). By Lemma 6(ii) and [21, Corollary 4(b)], we may assume that $f\in\mathcal{B}$. Now, (1.2) and (6.2) yield

$$\begin{aligned}\|f_r\|^2_{\mathrm{BMOA}}&\lesssim\sup_{a\in\mathbb{D}}\left(|f'(ra)|^2(1-|a|^2)^2\,r^2+\int_{\mathbb{D}}r^4|f''(rz)|^2(1-|z|^2)^2(1-|\varphi_a(z)|^2)\,dm(z)\right)\\&\lesssim\|f_r\|^2_{\mathcal{B}}+\sup_{a\in\mathbb{D}}\int_{\mathbb{D}}|f_r(z)-f_r(a)|^2\,|A(rz)|^2(1-|z|^2)^2(1-|\varphi_a(z)|^2)\,dm(z)\\&\qquad+\sup_{a\in\mathbb{D}}|f_r(a)|^2\int_{\mathbb{D}}|A(rz)|^2(1-|z|^2)^2(1-|\varphi_a(z)|^2)\,dm(z)\\&\lesssim\|f_r\|^2_{\mathcal{B}}+I_1+I_2\end{aligned}$$

with absolute comparison constants. By Carleson's theorem [8, Theorem 9.3], (6.1) and (6.3),

$$\begin{aligned}I_1&\lesssim\sup_{a\in\mathbb{D}}\int_{\mathbb{D}}|(f_r)_a(z)|^2\,\big|A(r\varphi_a(z))\big|^2\big(1-|\varphi_a(z)|^2\big)^3\,|\varphi_a'(z)|\,dm(z)\\&\lesssim\sup_{a\in\mathbb{D}}\left(\big\|(f_r)_a\big\|^2_{H^2}\cdot\sup_{b\in\mathbb{D}}\int_{\mathbb{D}}\big|A(r\varphi_a(z))\big|^2\big(1-|\varphi_a(z)|^2\big)^3|\varphi_a'(z)||\varphi_b'(z)|\,dm(z)\right)\\&\lesssim\|f_r\|^2_{\mathrm{BMOA}}\cdot\sup_{c\in\mathbb{D}}\int_{\mathbb{D}}|A(rz)|^2(1-|z|^2)^2\big(1-|\varphi_c(z)|^2\big)\,dm(z).\end{aligned}$$

Estimation of I_2 is easier. By [12, Corollary 5.3],

$$I_2 \lesssim \|f_r\|^2_{\mathrm{BMOA}} \cdot \sup_{a\in\mathbb{D}} \left(\log\frac{e}{1-|a|}\right)^2 \int_{\mathbb{D}} |A(rz)|^2(1-|z|^2)^2(1-|\varphi_a(z)|^2)\,dm(z).$$

If (2.4) is sufficiently small, then (6.4) implies that $\|f_r\|_{\mathrm{BMOA}}$ is uniformly bounded for $1/2 < r < 1$. By letting $r \to 1^-$, we conclude $f \in \mathrm{BMOA}$. □

The following example reveals that the coefficient condition in Theorem 3 allows solutions of (1.2) to be unbounded. Moreover, the same construction with $1 < \alpha < \infty$ illustrates that the finiteness of (2.4) is not enough to guarantee that all solutions of (1.2) are in BMOA. The same construction is applied in [21, Example 5(b)].

Example 2. Let $0 < \alpha \leq 1$, and define

$$A(z) = \frac{-\alpha}{(1-z)^2}\left((\alpha-1)\left(\log\frac{e}{1-z}\right)^{-2} + \left(\log\frac{e}{1-z}\right)^{-1}\right), \quad z \in \mathbb{D}.$$

Then $A \in \mathcal{H}(\mathbb{D})$, and (1.2) admits two linearly independent solutions

$$f_1(z) = \left(\log\frac{e}{1-z}\right)^{\alpha}, \quad f_2(z) = \left(\log\frac{e}{1-z}\right)^{\alpha} \int_0^z \left(\log\frac{e}{1-\zeta}\right)^{-2\alpha} d\zeta, \quad z \in \mathbb{D},$$

which are unbounded on positive real axis; see also [21, Example 5(b)]. We denote $A = -\alpha B_1 - \alpha(\alpha-1)B_2$, where $B_j(z) = (1-z)^{-2}(\log(e/(1-z)))^{-j}$ for $z \in \mathbb{D}$ and $j = 1, 2$. Since $|B_2(z)| \leq |B_1(z)|\,(\log(e/2))^{-1}$ for all $z \in \mathbb{D}$, and (4.2) holds for any $0 < a < 1$, we conclude (4.3). We point out that, for a sufficiently small α, the coefficient A satisfies the assumptions of Theorem 3 and hence all solutions of (1.2) are in BMOA.

The space VMOA consists of those $f \in H^2$ for which

$$\lim_{|a|\to 1^-} \|f_a\|^2_{H^2} = 0,$$

where f_a is the auxiliary function in the beginning of Section 6. Clearly, VMOA is a subspace of the little Bloch space $\mathcal{B}_0$. As Theorem 3 is motivated by [37, Theorem 3.1], the counterpart of the following result is [37, Theorem 3.6].

Theorem 7. *Let $A \in \mathcal{H}(\mathbb{D})$. If (2.4) is sufficiently small and*

$$\lim_{|a|\to 1^-} \left(\log\frac{e}{1-|a|}\right)^2 \int_{\mathbb{D}} |A(z)|^2(1-|z|^2)^2(1-|\varphi_a(z)|^2)\,dm(z) = 0,$$

then all solutions f of (1.2) satisfy $f \in \mathrm{VMOA}$.

The proof of Theorem 7 is omitted, since it is similar to the proof of Theorem 3. Note that the coefficient condition in Theorem 7 implies (7.11), and hence forces all solutions of (1.2) to be in the little Bloch space $\mathcal{B}_0$. See the end of Section 7 for more details.

7. Solutions in the Bloch and the little Bloch spaces

An integrable function $\omega : \mathbb{D} \to [0, \infty)$ is called a weight. The weight ω is said to be radial if $\omega(u) = \omega(|u|)$ for all $u \in \mathbb{D}$. For $0 < p < \infty$ and a weight ω, the weighted Bergman space A^p_ω consists of those $f \in \mathcal{H}(\mathbb{D})$ for which

$$\|f\|^p_{A^p_\omega} = \int_{\mathbb{D}} |f(u)|^p \omega(u)\,dm(u) < \infty.$$

For a radial weight ω, we define $\widehat{\omega}(u) = \int_{|u|}^1 \omega(r)\,dr$ for $u \in \mathbb{D}$. We denote $\omega \in \mathcal{D}$ whenever ω is radial and there exist constants $C = C(\omega) \geq 1$, $\alpha = \alpha(\omega) > 0$ and $\beta = \beta(\omega) \geq \alpha$ such that

$$C^{-1}\left(\frac{1-r}{1-t}\right)^{\alpha} \widehat{\omega}(t) \leq \widehat{\omega}(r) \leq C\left(\frac{1-r}{1-t}\right)^{\beta} \widehat{\omega}(t) \tag{7.1}$$

for all $0 \leq r \leq t < 1$. The existence of constants $\beta = \beta(\omega) > 0$ and $C = C(\omega) > 0$ for which the right-hand side inequality of (7.1) is satisfied is equivalent to the existence of a constant $K = K(\omega) \geq 1$ such that the doubling property $\widehat{\omega}(r) \leq K\,\widehat{\omega}((1+r)/2)$ holds for all $0 \leq r < 1$ [29, Lemma 1]. Moreover, the left-hand side inequality of (7.1) is equivalent to the existence of constants $K = K(\omega) > 1$ and $L = L(\omega) > 1$ such that $\widehat{\omega}(r) \geq K\,\widehat{\omega}(1-(1-r)/L)$ for all $0 \leq r < 1$, see [31] for more details.

Let $0 < p < \infty$ and ω be a radial weight. If $\widehat{\omega}(r) = 0$ for some $0 < r < 1$, then $A^p_\omega = \mathcal{H}(\mathbb{D})$. Let ω be a radial weight such that $\widehat{\omega}(r) > 0$ for all $0 \leq r < 1$. By standard estimates,

$$\|f\|^p_{A^p_\omega} \gtrsim M_p\left(\frac{1+r}{2}, f\right)^p \widehat{\omega}\left(\frac{1+r}{2}\right) \gtrsim M_\infty(r,f)^p(1-r)\,\widehat{\omega}\left(\frac{1+r}{2}\right), \quad 0 < r < 1,$$

where $M_p(r,f)$ denotes the H^p mean of f, and hence

$$|f(z)| \lesssim \frac{\|f\|_{A^p_\omega}}{\widehat{\omega}\left(\frac{1+|z|}{2}\right)^{1/p}(1-|z|)^{1/p}}, \quad z \in \mathbb{D}. \tag{7.2}$$

We will concentrate on the case $p = 2$. By (7.2), the norm convergence in A^2_ω implies the uniform convergence on compact subsets of $\mathbb{D}$, and consequently each point evaluation $L_\zeta(f) = f(\zeta)$ is a bounded linear functional in the Hilbert space A^2_ω. Hence, there exist unique reproducing kernels $B^\omega_\zeta \in A^2_\omega$ with $\|L_\zeta\| = \|B^\omega_\zeta\|_{A^2_\omega}$ such that

$$f(\zeta) = \langle f, B^\omega_\zeta\rangle_{A^2_\omega} = \int_{\mathbb{D}} f(u)\overline{B^\omega_\zeta(u)}\omega(u)\,dm(u), \quad f \in A^2_\omega. \tag{7.3}$$

Moreover, the normalized monomials $(2\,\omega_{2n+1})^{-1/2}\,z^n$, for $n \in \mathbb{N}\cup\{0\}$, form the standard orthonormal basis of A^2_ω, and hence

$$B^\omega_\zeta(u) = \sum_{n=0}^{\infty} \frac{(u\overline{\zeta})^n}{2\,\omega_{2n+1}}, \quad u, \zeta \in \mathbb{D}; \tag{7.4}$$

see [41, Theorem 4.19] for details in the classical case. Here $\omega_x = \int_0^1 r^x\omega(r)\,dr$ for $1 \leq x < \infty$. Weight ω is called normalized if $\omega_1 = 1/2$, which implies that $\omega(\mathbb{D}) = \int_{\mathbb{D}}\omega(u)\,dm(u) = 2\omega_1 = 1$.

We begin with a lemma which shows that the derivative of B^ω_ζ is closely related to the reproducing kernel of another Bergman space with a suitably chosen weight. For example, $B^\omega_\zeta(u) = (1-u\overline{\zeta})^{-2-\alpha}$ is the reproducing kernel corresponding to the standard weight $\omega(u) = (\alpha+1)(1-|u|^2)^\alpha$, $\alpha > -1$, while $(B^\omega_\zeta)'(u) = (2+\alpha)\overline{\zeta}(1-u\overline{\zeta})^{-3-\alpha}$ is related to the reproducing kernel of the Bergman space with the weight $\widetilde{\omega}(u) = (1-|u|^2)^{\alpha+1}$. In general, we define

$$\widetilde{\omega}(u) = 2\int_{|u|}^1 \omega(r)r\,dr, \quad u \in \mathbb{D},$$

for any radial weight ω.

Lemma 8. *If ω is radial then $(B^\omega_\zeta)'(u) = \overline{\zeta}\,B^{\widetilde{\omega}}_\zeta(u)$ for $u, \zeta \in \mathbb{D}$.*

Proof. It is clear that representations (7.4) exist for both B^ω_ζ and $B^{\widetilde{\omega}}_\zeta$. By Fubini's theorem,

$$\widetilde{\omega}_{2n+1} = 2\int_0^1 \omega(s)s\int_0^s r^{2n+1}\,dr\,ds = \frac{\omega_{2n+3}}{n+1}, \quad n \in \mathbb{N}\cup\{0\},$$

and hence

$$(B^\omega_\zeta)'(u) = \overline{\zeta}\sum_{n=0}^{\infty}\frac{(n+1)(u\overline{\zeta})^n}{2\,\omega_{2n+3}} = \overline{\zeta}\,B^{\widetilde{\omega}}_\zeta(u), \quad u, \zeta \in \mathbb{D}.$$

This proves the assertion. □

The following auxiliary result is well-known to experts. For a radial weight ω, we define

$$\omega^\star(u) = \int_{|u|}^1 \log \frac{r}{|u|}\, \omega(r)\, r\, dr, \quad u \in \mathbb{D} \setminus \{0\}.$$

Lemma 9. *If $f, g \in H^2$, then*

$$\frac{1}{2\pi}\int_0^{2\pi} f(e^{it})\overline{g(e^{it})}\, dt = 2\int_{\mathbb{D}} f'(u)\overline{g'(u)} \log\frac{1}{|u|}\, dm(u) + f(0)\overline{g(0)}. \tag{7.5}$$

Moreover, if $f, g \in \mathcal{H}(\mathbb{D})$ and ω is a normalized radial weight, then

$$\langle f, g\rangle_{A^2_\omega} = 4\,\langle f', g'\rangle_{A^2_{\omega^\star}} + f(0)\overline{g(0)}.$$

Proof. Identity (7.5) is a special case of [41, Theorem 9.9]. Let $f, g \in \mathcal{H}(\mathbb{D})$. By (7.5),

$$\frac{1}{\pi}\int_0^{2\pi} f(re^{it})\overline{g(re^{it})}\, dt = 4\int_{D(0,r)} f'(u)\overline{g'(u)} \log\frac{r}{|u|}\, dm(u) + 2f(0)\overline{g(0)}.$$

The assertion follows by integrating both sides with respect to the measure $\omega(r)r\, dr$ and using Fubini's theorem. □

Recall that the Bloch space $\mathcal{B}$ consists of those $f \in \mathcal{H}(\mathbb{D})$ for which

$$\|f\|_{\mathcal{B}} = \sup_{z\in\mathbb{D}} |f'(z)|(1-|z|^2) < \infty.$$

Theorem 10. *Let $\omega \in \mathcal{D}$ be normalized, and $A \in \mathcal{H}(\mathbb{D})$ such that*

$$\limsup_{r\to 1^-} \sup_{z\in\mathbb{D}} (1-|z|^2) \int_{\mathbb{D}} \left| \int_0^z \overline{(B^\omega_\zeta)'(u)} A(r\zeta)\, d\zeta \right| \frac{\omega^\star(u)}{1-|u|^2}\, dm(u) < \frac{1}{4}. \tag{7.6}$$

Then every solution f of (1.2) satisfies $f \in \mathcal{B}$, and

$$\|f\|_{\mathcal{B}} \le \frac{1}{1-4\,X_{\mathcal{B}}(A)} \left(|f(0)| \sup_{z\in\mathbb{D}} (1-|z|^2) \left| \int_0^z A(\zeta)\, d\zeta \right| + |f'(0)| \right),$$

where

$$X_{\mathcal{B}}(A) = \sup_{z\in\mathbb{D}} (1-|z|^2) \int_{\mathbb{D}} \left| \int_0^z \overline{(B^\omega_\zeta)'(u)} A(\zeta)\, d\zeta \right| \frac{\omega^\star(u)}{1-|u|^2}\, dm(u) < \frac{1}{4}.$$

Proof. Observe that $\omega^\star(u)/(1-|u|^2) \asymp \widetilde{\omega}(u)$ as $|u| \to 1^-$, since $\omega \in \mathcal{D}$ by the hypothesis. For fixed $z \in \mathbb{D}$, Fubini's theorem and Lemma 8 yield

$$\begin{aligned}
&\limsup_{r\to 1^-} (1-|z|^2) \int_{\mathbb{D}} \left| \int_0^z \overline{(B^\omega_\zeta)'(u)} A(r\zeta)\, d\zeta \right| \frac{\omega^\star(u)}{1-|u|^2}\, dm(u) \\
&\quad \gtrsim (1-|z|^2) \int_{\mathbb{D}} \left| \int_0^z \overline{(B^\omega_\zeta)'(u)} A(\zeta)\, d\zeta \right| \widetilde{\omega}(u)\, dm(u) \\
&\quad \ge (1-|z|^2) \left| \int_0^z \langle 1, B^{\widetilde{\omega}}_\zeta\rangle_{A^2_\omega}\, A(\zeta)\zeta\, d\zeta \right| \ge (1-|z|^2) \left| \int_0^z A(\zeta)\zeta\, d\zeta \right|,
\end{aligned} \tag{7.7}$$

and it follows that $A \in H^\infty_2$. Note that the use of the reproducing formula could be avoided by a straightforward integration.

Let f be any solution of (1.2). Then

$$f_r'(z) = -\int_0^z f_r(\zeta) r^2 A(r\zeta)\, d\zeta + f_r'(0), \quad z \in \mathbb{D}. \tag{7.8}$$

The reproducing formula (7.3) and Fubini's theorem imply

$$\begin{aligned}
f_r'(z) &= -\int_0^z \left(\int_{\mathbb{D}} f_r(u)\overline{B^\omega_\zeta(u)}\omega(u)\, dm(u) \right) r^2 A(r\zeta)\, d\zeta + f_r'(0) \\
&= -\int_{\mathbb{D}} f_r(u) \left(\int_0^z \overline{B^\omega_\zeta(u)} r^2 A(r\zeta)\, d\zeta \right) \omega(u)\, dm(u) + f_r'(0), \quad z \in \mathbb{D},
\end{aligned}$$

from which the second part of Lemma 9 yields

$$f_r'(z) = -4\int_{\mathbb{D}} f_r'(u)\left(\int_0^z \overline{(B_\zeta^\omega)'(u)} r^2 A(r\zeta)\,d\zeta\right)\omega^\star(u)\,dm(u) - f_r(0)\int_0^z r^2 A(r\zeta)\,d\zeta + f_r'(0), \quad z\in\mathbb{D}.$$

It follows that

$$\|f_r\|_{\mathcal{B}} \le 4\,\|f_r\|_{\mathcal{B}} \sup_{z\in\mathbb{D}}(1-|z|^2)\int_{\mathbb{D}}\left|\int_0^z \overline{(B_\zeta^\omega)'(u)}A(r\zeta)\,d\zeta\right|\frac{\omega^\star(u)}{1-|u|^2}\,dm(u) + |f(0)|\sup_{z\in\mathbb{D}}(1-|z|^2)\left|\int_0^z A(r\zeta)\,d\zeta\right| + |f'(0)|, \quad 0<r<1.$$

We deduce $f\in\mathcal{B}$ by re-organizing the terms and letting $r\to 1^-$.

Since $f\in\mathcal{B}$, we know that $M_\infty(r,f)\lesssim \log(e/(1-r))$ for $0<r<1$. Hence, for any $0<p<\infty$,

$$\|f\|_{A^p_\omega}^p \lesssim \widehat{\omega}(0) + p\int_0^1 \left(\log\frac{e}{1-r}\right)^{p-1}\frac{1}{(1-r)^{1-\alpha}}\,dr<\infty$$

by partial integration and (7.1); see also [27, Proposition 6.1]. Now that $f\in\mathcal{B}\subset A^2_\omega$, we may repeat the proof from the beginning with $r=1$ to deduce the second part of the assertion. □

Remark 2. The proof of Theorem 10 shows that, in order to conclude $f\in\mathcal{B}$, it suffices to take the supremum in (7.6) over any annulus $R<|z|<1$ instead of $\mathbb{D}$.

We apply an operator theoretic argument to study the sharpness of Theorem 10. Let

$$I(A,\omega) = \limsup_{r\to 1^-}\sup_{z\in\mathbb{D}}(1-|z|^2)\int_{\mathbb{D}}\left|\int_0^z \overline{(B_\zeta^\omega)'(u)}A(r\zeta)\,d\zeta\right|\frac{\omega^\star(u)}{1-|u|^2}\,dm(u)$$

denote the left-hand side of (7.6), for short.

Theorem 11. *Let $\omega\in\mathcal{D}$ be normalized and $A\in\mathcal{H}(\mathbb{D})$. Then the following statements are equivalent:*

(i) $A\in\mathcal{L}^1$;
(ii) $I(A,\omega)<\infty$;
(iii) *the operator $S_A:\mathcal{B}\to\mathcal{B}$ is bounded.*

Proof. (i) $\Longrightarrow$ (ii): Observe that $\omega^\star(u)/(1-|u|^2)\asymp\widehat{\omega}(u)$ as $|u|\to 1^-$. By Fubini's theorem,

$$I(A,\omega)\lesssim \limsup_{r\to 1^-}\sup_{z\in\mathbb{D}}(1-|z|^2)\int_0^z |A(r\zeta)|\left(\int_{\mathbb{D}}\left|(B_\zeta^\omega)'(u)\right|\widehat{\omega}(u)\,dm(u)\right)|d\zeta|,$$

where

$$\int_{\mathbb{D}}\left|(B_\zeta^\omega)'(u)\right|\widehat{\omega}(u)\,dm(u)\lesssim\int_0^{|\zeta|}\frac{\widehat{\widehat{\omega}}(t)\,dt}{\widehat{\omega}(t)(1-t)^2}\asymp\int_0^{|\zeta|}\frac{dt}{1-t^2}=\frac{1}{2}\log\frac{1+|\zeta|}{1-|\zeta|},\quad \zeta\in\mathbb{D},$$

by [30, Theorem 1], Fubini's theorem and (7.1). It follows that $I(A,\omega)\lesssim\|A\|_{\mathcal{L}^1}<\infty$.

(ii) $\Longrightarrow$ (iii): This implication follows by an argument similar to the proof of Theorem 10. As in (7.7), we deduce

$$\sup_{z\in\mathbb{D}}(1-|z|^2)\int_{\mathbb{D}}\left|\int_0^z\overline{(B_\zeta^\omega)'(u)}A(\zeta)\,d\zeta\right|\frac{\omega^\star(u)}{1-|u|^2}\,dm(u)\le I(A,\omega)<\infty,$$

and $A \in H^\infty_2$. Let $f \in \mathcal{B} \subset A^2_\omega$. The reproducing formula (7.3), Fubini's theorem and Lemma 9 imply

$$\begin{aligned}\big\|S_A(f)\big\|_{\mathcal{B}} &= \sup_{z\in\mathbb{D}} (1-|z|^2)\left|\int_0^z f(\zeta)A(\zeta)\,d\zeta\right| \lesssim \|f\|_{\mathcal{B}}\, I(A,\omega) + |f(0)|\cdot\|A\|_{H^\infty_2} \\ &\lesssim \big(\|f\|_{\mathcal{B}} + |f(0)|\big)\, I(A,\omega),\end{aligned}$$

and hence we deduce (iii).

(iii) $\Longrightarrow$ (i): By the assumption, there exists a constant $C>0$ such that

$$\sup_{z\in\mathbb{D}} |f(z)|\,|A(z)|(1-|z|^2)^2 = \big\|S_A(f)''\big\|_{H^\infty_2} \lesssim \big\|S_A(f)\big\|_{\mathcal{B}} \le C\big(\|f\|_{\mathcal{B}} + |f(0)|\big) \tag{7.9}$$

for any $f \in \mathcal{B}$. Consider the family of test functions

$$f_\zeta(z) = \log\frac{e}{1-\overline{\zeta}z}, \quad z,\zeta\in\mathbb{D},$$

for which $\sup_{\zeta\in\mathbb{D}}\|f_\zeta\|_{\mathcal{B}} \le 2$. By (7.9),

$$\left|\log\frac{e}{1-\overline{\zeta}z}\right| |A(z)|(1-|z|^2)^2 \le 3C, \quad z,\zeta\in\mathbb{D},$$

which gives (i) for $\zeta = z$. □

A close look at the proof of Theorem 11 implies

$$I(A,w) \asymp \sup_{z\in\mathbb{D}} (1-|z|^2)\int_{\mathbb{D}}\left|\int_0^z \overline{(B^\omega_\zeta)'(u)}A(\zeta)\,d\zeta\right| \frac{\omega^\star(u)}{1-|u|^2}\,dm(u).$$

We obtain the following consequence of Theorem 10.

Corollary 12. *Let $\omega \in \mathcal{D}$ be normalized, and $A \in \mathcal{H}(\mathbb{D})$ such that*

$$\sup_{z\in\mathbb{D}} (1-|z|^2)\int_{\mathbb{D}}\left|\int_0^z \overline{(B^\omega_\zeta)'(u)}A(\zeta)\,d\zeta\right| \frac{\omega^\star(u)}{1-|u|^2}\,dm(u) \tag{7.10}$$

is sufficiently small. Then every solution of (1.2) *belongs to $\mathcal{B}$.*

Remark 3. In order to conclude that all solutions of (1.2) are in $\mathcal{B}$, it suffices to take the supremum in (7.10) over any annulus $R<|z|<1$ instead of $\mathbb{D}$.

The little Bloch space $\mathcal{B}_0$ consists of those $f\in\mathcal{H}(\mathbb{D})$ for which

$$\lim_{|z|\to 1^-} |f'(z)|(1-|z|^2) = 0.$$

The following result is a counterpart of Theorem 10 concerning the little Bloch space.

Theorem 13. *Let $\omega \in \mathcal{D}$ be normalized, and $A \in \mathcal{H}(\mathbb{D})$ such that*

$$\lim_{|z|\to 1^-} (1-|z|^2)\int_{\mathbb{D}}\left|\int_0^z \overline{(B^\omega_\zeta)'(u)}A(\zeta)\,d\zeta\right| \frac{\omega^\star(u)}{1-|u|^2}\,dm(u) = 0.$$

Then every solution of (1.2) *belongs to $\mathcal{B}_0$.*

Proof. As in (7.7), we conclude

$$\lim_{|z|\to 1^-} (1-|z|^2)\left|\int_0^z A(\zeta)\zeta\,d\zeta\right| = 0.$$

By the assumption and Remark 3, it follows that each solution f of (1.2) satisfies $f\in\mathcal{B}\subset A^2_\omega$. As in the proof of Theorem 10, we have

$$\begin{aligned}(1-|z|^2)|f'(z)| \le 4\,\|f\|_{\mathcal{B}}\,(1-|z|^2)\int_{\mathbb{D}}\left|\int_0^z \overline{(B^\omega_\zeta)'(u)}A(\zeta)\,d\zeta\right| \frac{\omega^\star(u)}{1-|u|^2}\,dm(u) \\ + |f(0)|\,(1-|z|^2)\left|\int_0^z A(\zeta)\,d\zeta\right| + (1-|z|^2)|f'(0)|, \quad z\in\mathbb{D}.\end{aligned}$$

The assertion follows. □

If $A \in \mathcal{H}(\mathbb{D})$ and

$$\lim_{|z|\to 1^-} |A(z)|(1-|z|^2)^2 \log \frac{e}{1-|z|} = 0, \tag{7.11}$$

then every solution of (1.2) belongs to $\mathcal{B}_0$. Actually, $f \in \mathcal{B}$ by Remark 3. Therefore

$$f''(z) = -A(z) \int_{\mathbb{D}} \frac{f(u)}{(1-\overline{u}z)^2}\, dm(u), \quad z \in \mathbb{D}.$$

By applying Lemma 9 twice, we obtain

$$|f''(z)| \lesssim |A(z)| \left(|f(0)| + |f'(0)| + \|f''\|_{H^\infty_2} \int_{\mathbb{D}} \frac{(1-|u|^2)^2}{|1-\overline{u}z|^4}\, dm(u) \right), \quad z \in \mathbb{D}.$$

Since $f \in \mathcal{B}$, we deduce $f'' \in H^\infty_2$, and hence the argument above shows that $f \in \mathcal{B}_0$ by [41, Lemma 3.10 and Theorem 5.13].

The coefficient condition (7.11), which forces all solutions of (1.2) to be in $\mathcal{B}_0$, is sharp in the sense that it cannot be replaced by $A \in \mathcal{L}^1$. Indeed, the function $f(z) = \log(e/(1-z)) \in \mathcal{B} \setminus \mathcal{B}_0$ is a solution of (1.2) for

$$A(z) = \frac{-1}{(1-z)^2 \log(e/(1-z))}, \quad z \in \mathbb{D}.$$

8. Solutions of bounded and vanishing mean oscillation — parallel results

In this section, we consider two coefficient estimates, which are derived from the representation (5.1). These estimates give sufficient conditions for all solutions of (1.2) to be in BMOA or VMOA. Recall that, by (6.2) and (6.3), the measure $d\mu_f(z) = |f'(z)|^2(1-|z|^2)\, dm(z)$ satisfies

$$\|\mu_f\|_{\text{Carleson}} \lesssim \|f\|^2_{\text{BMOA}}. \tag{8.1}$$

Actually, $f \in \text{BMOA}$ if and only if μ_f is a Carleson measure [11, p. 231].

Theorem 14. *Let $A \in \mathcal{H}(\mathbb{D})$. If*

$$\limsup_{r\to 1^-} \sup_{a\in\mathbb{D}} \int_{\mathbb{D}} \left(\frac{1}{2\pi} \int_0^{2\pi} \left| \int_0^z \frac{A(r\zeta)\, d\zeta}{1-e^{-it}\zeta} \right| dt \right)^2 (1-|\varphi_a(z)|^2)\, dm(z) \tag{8.2}$$

is sufficiently small, then all solutions of (1.2) *belong to* BMOA.

Proof. By applying (5.1) to $g \equiv 1$, we obtain

$$\left| \int_0^z A(r\zeta)\, d\zeta \right| = \left| \frac{1}{2\pi} \int_0^{2\pi} \int_0^z \frac{A(r\zeta)\, d\zeta}{1-e^{-it}\zeta}\, dt \right| \le \frac{1}{2\pi} \int_0^{2\pi} \left| \int_0^z \frac{A(r\zeta)\, d\zeta}{1-e^{-it}\zeta} \right| dt, \tag{8.3}$$

for $0 \le r \le 1$ and $z \in \mathbb{D}$. By (6.2) and (8.2), any second primitive of A belongs to BMOA.

Let f be a solution of (1.2). Then f_r is analytic in $\overline{\mathbb{D}}$ and satisfies $f_r''(\zeta) + r^2 A(r\zeta) f_r(\zeta) = 0$. We deduce (7.8). By (5.1) and Fubini's theorem,

$$\begin{aligned} f_r'(z) &= -\frac{1}{2\pi} \int_0^{2\pi} f_r(e^{it}) \int_0^z \frac{r^2 A(r\zeta)}{1-e^{-it}\zeta}\, d\zeta\, dt + f_r'(0) \\ &= -\frac{r^2}{2\pi} \int_0^{2\pi} f_r(e^{it}) \overline{g_{r,z}(e^{it})}\, dt + f_r'(0), \quad z \in \mathbb{D}, \end{aligned}$$

where

$$g_{r,z}(w) = \overline{\int_0^z \frac{A(r\zeta)}{1-\overline{w}\zeta}\, d\zeta}, \quad w \in \mathbb{D}. \tag{8.4}$$

Since $f_r, g_{r,z} \in H^2$, Lemma 9 implies

$$\frac{1}{2\pi} \int_0^{2\pi} f_r(e^{it}) \overline{g_{r,z}(e^{it})}\, dt = 2 \int_{\mathbb{D}} f_r'(w) \overline{g_{r,z}'(w)} \log \frac{1}{|w|}\, dm(w) + f_r(0) \overline{g_{r,z}(0)}.$$

We deduce

$$|f_r'(z)|^2 \le 8\left|\int_{\mathbb{D}} f_r'(w)\overline{g_{r,z}'(w)}\log\frac{1}{|w|}\,dm(w)\right|^2 + 2\left|f_r(0)\overline{g_{r,z}(0)} - f_r'(0)\right|^2, \quad z\in\mathbb{D}.$$

By the Hardy-Stein-Spencer formula

$$\int_{\mathbb{D}} \frac{|g_{r,z}'(w)|^2}{|g_{r,z}(w)|}\log\frac{1}{|w|}\,dm(w) \le 2\,\|g_{r,z}\|_{H^1},$$

and hence by (8.1) and Carleson's theorem [8, Theorem 9.3], there exist absolute constants $0<C<\infty$ and $0<C'<\infty$ such that

$$\begin{aligned}\left|\int_{\mathbb{D}} f_r'(w)\overline{g_{r,z}'(w)}\log\frac{1}{|w|}\,dm(w)\right|^2 &\le \int_{\mathbb{D}} \frac{|g_{r,z}'(w)|^2}{|g_{r,z}(w)|}\log\frac{1}{|w|}\,dm(w)\\ &\qquad\cdot\int_{\mathbb{D}} |g_{r,z}(w)||f_r'(w)|^2\log\frac{1}{|w|}\,dm(w)\\ &\le 2\,\|g_{r,z}\|_{H^1}C'\,\|\mu_{f_r}\|_{\mathrm{Carleson}}\,\|g_{r,z}\|_{H^1}\\ &\le 2C\,\|g_{r,z}\|_{H^1}^2\|f_r\|_{\mathrm{BMOA}}^2.\end{aligned}$$

We have $|f_r'(z)|^2 \le 16C\,\|g_{r,z}\|_{H^1}^2\|f_r\|_{\mathrm{BMOA}}^2 + 4\,|f_r(0)|^2|g_{r,z}(0)|^2 + 4\,|f_r'(0)|^2$ for $z\in\mathbb{D}$, and by (6.2),

$$\begin{aligned}\|f_r\|_{\mathrm{BMOA}}^2 \le 64C\,\|f_r\|_{\mathrm{BMOA}}^2 &\sup_{a\in\mathbb{D}}\int_{\mathbb{D}}\|g_{r,z}\|_{H^1}^2(1-|\varphi_a(z)|^2)\,dm(z)\\ &+ 16\,|f_r(0)|^2\sup_{a\in\mathbb{D}}\int_{\mathbb{D}}|g_{r,z}(0)|^2(1-|\varphi_a(z)|^2)\,dm(z) + 16\,|f_r'(0)|^2.\end{aligned}$$

By re-organizing terms and letting $r\to 1^-$, the assertion follows. □

Remark 4. The proof of Theorem 14 shows that, in order to conclude $f\in\mathrm{BMOA}$, it suffices to take the supremum in (8.2) over any annulus $R<|z|<1$ instead of $\mathbb{D}$.

Theorem 15. *Let $A\in\mathcal{H}(\mathbb{D})$. If* (8.2) *is sufficiently small and*

$$\lim_{|a|\to 1^-}\int_{\mathbb{D}}\left(\frac{1}{2\pi}\int_0^{2\pi}\left|\int_0^z \frac{A(\zeta)d\zeta}{1-e^{-it}\zeta}\right|dt\right)^2(1-|\varphi_a(z)|^2)\,dm(z) = 0,$$

then every solution of (1.2) *belongs to* VMOA.

Proof. First, by the assumption and (8.3), any second primitive of A belongs to VMOA. Let f be any solution of (1.2). By the assumption and Theorem 14, we have $f\in\mathrm{BMOA}$. As in the proof of Theorem 14, we obtain

$$|f'(z)|^2 \lesssim \|g_{1,z}\|_{H^1}^2\|f\|_{\mathrm{BMOA}}^2 + |g_{1,z}(0)|^2|f(0)|^2 + |f'(0)|^2, \quad z\in\mathbb{D},$$

where $g_{1,z}$ is the function in (8.4). Hence, by (6.2),

$$\begin{aligned}\|f_a\|_{H^2}^2 \lesssim \|f\|_{\mathrm{BMOA}}^2 &\int_{\mathbb{D}}\|g_{1,z}\|_{H^1}^2(1-|\varphi_a(z)|^2)\,dm(z)\\ &+ |f(0)|^2\int_{\mathbb{D}}|g_{1,z}(0)|^2\,(1-|\varphi_a(z)|^2)\,dm(z)\\ &+ |f'(0)|^2(1-|a|^2)\int_{\mathbb{D}}\frac{1-|z|^2}{|1-\overline{a}z|^2}\,dm(z).\end{aligned}$$

The assertion follows by letting $|a|\to 1^-$. □

9. Hardy spaces

For $0 < p < \infty$, the Hardy space H^p consists of those $f \in \mathcal{H}(\mathbb{D})$ for which

$$\|f\|_{H^p}^p = \sup_{0\leq r<1} \frac{1}{2\pi}\int_0^{2\pi} |f(re^{i\theta})|^p \, d\theta < \infty.$$

Proof of Theorem 4. The case $p = 2$ follows from the Littlewood-Paley identity by standard estimates, and if $k = 1$ then much more is true, see [26].

The following arguments rely on the representation (5.3) and on an application of the non-tangential maximal function (5.4). For $z \in \mathbb{D}$, let $I(z) = \{\zeta \in \mathbb{T} : z \in \Gamma(\zeta)\}$ and note that its Euclidean arc length satisfies $|I(z)| \asymp 1 - |z|^2$ for $z \in \mathbb{D}$.

(i) We proceed to prove the following preliminary estimate. If $0 < p < 2$, $k \in \mathbb{N}$ and $0 < r < 1$, then

$$\|f_r\|_{H^p}^p \lesssim \int_{\mathbb{D}} |f_r(z)|^{p-2}|f_r^{(k)}(z)|^2(1-|z|^2)^{2(k-1)+1}\, dm(z) + \frac{\left(\sum_{j=0}^{k-1}|f^{(j)}(0)|^p\right)^{2/p}}{\|f_r\|_{H^p}^{2-p}} \tag{9.1}$$

for all $f \in \mathcal{H}(\mathbb{D})$, $f \not\equiv 0$. Write $d\mu_r(z) = |f_r^{(k)}(z)|^2(1-|z|^2)^{2(k-1)}\, dm(z)$ for short. Fubini's theorem and Hölder's inequality (with indices $2/(2-p)$ and $2/p$) yield

$$\begin{aligned}
\|f_r\|_{H^p}^p &\asymp \int_{\mathbb{T}} \left(\int_{\Gamma(\zeta)} d\mu_r(z)\right)^{\frac{p}{2}} |d\zeta| + \sum_{j=0}^{k-1}|f_r^{(j)}(0)|^p \\
&\leq \int_{\mathbb{T}} f_r^\star(\zeta)^{(2-p)\frac{p}{2}} \left(\int_{\Gamma(\zeta)} |f_r(z)|^{p-2}\, d\mu_r(z)\right)^{\frac{p}{2}} |d\zeta| + \sum_{j=0}^{k-1}|f^{(j)}(0)|^p \\
&\leq \left(\int_{\mathbb{T}} f_r^\star(\zeta)^p\, |d\zeta|\right)^{\frac{2-p}{2}} \left(\int_{\mathbb{T}}\int_{\Gamma(\zeta)} |f_r(z)|^{p-2}\, d\mu_r(z)|d\zeta|\right)^{\frac{p}{2}} + \sum_{j=0}^{k-1}|f^{(j)}(0)|^p \\
&\lesssim \|f_r\|_{H^p}^{p(1-\frac{p}{2})} \left(\int_{\mathbb{D}} |f_r(z)|^{p-2}(1-|z|^2)\, d\mu_r(z)\right)^{\frac{p}{2}} + \sum_{j=0}^{k-1}|f^{(j)}(0)|^p,
\end{aligned}$$

where the last inequality follows from [11, pp. 55–56]. Estimate (9.1) follows by reorganizing the terms.

By a change of variable, we get

$$\begin{aligned}
&\int_{\mathbb{D}} |f_r(z)|^{p-2}|f_r^{(k)}(z)|^2(1-|z|^2)^{2(k-1)+1}\, dm(z) \\
&\qquad \leq \int_{\mathbb{D}} |f(z)|^{p-2}|f^{(k)}(z)|^2\left(1-|z|^2\right)^{2k-1}\, dm(z).
\end{aligned} \tag{9.2}$$

By means of (9.1) we conclude that, if (9.2) is finite then $f \in H^p$ and

$$\|f\|_{H^p}^p \lesssim \int_{\mathbb{D}} |f(z)|^{p-2}|f^{(k)}(z)|^2\left(1-|z|^2\right)^{2k-1}\, dm(z) + \frac{\left(\sum_{j=0}^{k-1}|f^{(j)}(0)|^p\right)^{2/p}}{\|f\|_{H^p}^{2-p}}. \tag{9.3}$$

Cauchy's integral formula, and the estimate $|f(z)| \lesssim \|f\|_{H^p}(1-|z|^2)^{-1/p}$ for $z \in \mathbb{D}$ [8, p. 36], give $|f^{(j)}(0)|^2 \lesssim \|f\|_{H^p}^{2-p}\cdot|f^{(j)}(0)|^p$ for $j = 0, 1, \ldots, k-1$, which implies

$$\left(\sum_{j=0}^{k-1}|f^{(j)}(0)|^p\right)^{2/p} \lesssim \sum_{j=0}^{k-1}|f^{(j)}(0)|^2 \lesssim \|f\|_{H^p}^{2-p}\sum_{j=0}^{k-1}|f^{(j)}(0)|^p. \tag{9.4}$$

Now (9.3) and (9.4) prove (2.9).

(ii) Let $2 < p < \infty$. We may assume that $f \in H^p$, for otherwise there is nothing to prove. Write $q = p - 2$ and $d\mu(z) = |f^{(k)}(z)|^2 (1-|z|^2)^{2(k-1)+1}\, dm(z)$, for short. Fubini's theorem, Hölder's inequality (with indices p/q and $p/(p-q)$) and [11, pp. 55–56] yield

$$\begin{aligned}
\int_{\mathbb{D}} |f(z)|^q \, d\mu(z) &\asymp \int_{\mathbb{D}} \left(\int_{I(z)} |d\zeta| \right) \frac{|f(z)|^q}{1-|z|^2} \, d\mu(z) = \int_{\mathbb{T}} \int_{\Gamma(\zeta)} \frac{|f(z)|^q}{1-|z|^2} \, d\mu(z) \, |d\zeta| \\
&\leq \left(\int_{\mathbb{T}} f^\star(\zeta)^p \, |d\zeta| \right)^{\frac{q}{p}} \left(\int_{\mathbb{T}} \left(\int_{\Gamma(\zeta)} \frac{d\mu(z)}{1-|z|^2} \right)^{\frac{p}{p-q}} |d\zeta| \right)^{\frac{p-q}{p}} \\
&\lesssim \|f\|_{H^p}^{p-2} \left(\int_{\mathbb{T}} \left(\int_{\Gamma(\zeta)} |f^{(k)}(z)|^2 (1-|z|^2)^{2(k-1)} \, dm(z) \right)^{\frac{p}{2}} |d\zeta| \right)^{\frac{2}{p}} \\
&\lesssim \|f\|_{H^p}^{p-2} \left(\|f\|_{H^p}^p - \sum_{j=0}^{k-1} |f^{(j)}(0)|^p \right)^{\frac{2}{p}} \lesssim \|f\|_{H^p}^p,
\end{aligned}$$

and the assertion of (ii) follows.

(iii) If $f \in \mathcal{H}(\mathbb{D})$ is uniformly locally univalent, then $\sup_{z\in\mathbb{D}} |f''(z)/f'(z)|\,(1-|z|^2)$ is bounded by a constant depending on δ [39, Theorem 2]. Here $0 < \delta \leq 1$ is a constant such that f is univalent in each pseudo-hyperbolic disc $\Delta(z,\delta)$ for $z \in \mathbb{D}$. Since

$$\left(\frac{f^{(k)}}{f'} \right)' = \frac{f^{(k+1)}}{f'} - \frac{f''}{f'} \cdot \frac{f^{(k)}}{f'}, \quad k \in \mathbb{N},$$

we conclude $\|f^{(k+1)}/f'\|_{H^\infty_k} < \infty$ for $k \in \mathbb{N}$ by induction. By means of the Hardy-Stein-Spencer formula, we deduce

$$\begin{aligned}
&\int_{\mathbb{D}} |f(z)|^{p-2} |f^{(k)}(z)|^2 (1-|z|^2)^{2k-1} \, dm(z) \\
&\quad \lesssim \left\| \frac{f^{(k)}}{f'} \right\|_{H^\infty_{k-1}}^2 \int_{\mathbb{D}} |f(z)|^{p-2} |f'(z)|^2 \log \frac{1}{|z|} \, dm(z) \lesssim \|f\|_{H^p}^p,
\end{aligned}$$

where the comparison constant depends on δ and p. This completes the proof of Theorem 4. □

9.1. **A class of functions for which Question 1 has an affirmative answer.** If $f \in \mathcal{H}(\mathbb{D})$ is non-vanishing, then $g = f^{(p-2)/2} f' \in \mathcal{H}(\mathbb{D})$ and $g' = \frac{p-2}{2} f^{\frac{p-4}{2}} (f')^2 + f^{\frac{p-2}{2}} f''$. The Hardy-Stein-Spencer formula (2.7) implies

$$\|f\|_{H^p}^p \leq |f(0)|^p + C_1\, p^2 \int_{\mathbb{D}} |g(z)|^2 (1-|z|^2) \, dm(z), \tag{9.5}$$

where $0 < C_1 < \infty$ is an absolute constant. By standard estimates, there exists another absolute constant $0 < C_2 < \infty$ such that

$$\int_{\mathbb{D}} |g(z)|^2 (1-|z|^2) \, dm(z) \leq C_2 \left(|g(0)|^2 + \int_{\mathbb{D}} |g'(z)|^2 (1-|z|^2)^3 \, dm(z) \right).$$

By (9.5), we deduce

$$\begin{aligned}
\|f\|_{H^p}^p \leq |f(0)|^p + C_1 C_2\, p^2 \left\| \frac{f'}{f} \right\|_{H^\infty_1}^{2-p} |f'(0)|^p + 2\, C_1 C_2\, (p-2)^2 \left\| \frac{f'}{f} \right\|_{H^\infty_1}^2 \|f\|_{H^p}^p \\
+ 2 C_1 C_2\, p^2 \int_{\mathbb{D}} |f(z)|^{p-2} |f''(z)|^2 (1-|z|^2)^3 \, dm(z).
\end{aligned}$$

In conclusion, if $f \in \mathcal{H}(\mathbb{D})$ is non-vanishing and $\|f'/f\|_{H^\infty_1} = \|\log f\|_{\mathcal{B}}$ is sufficiently small, then (2.8) holds with $C(p) \asymp p^2$ as $p \to 0^+$.

9.2. **Applications to differential equations.** Theorem 4 induces an alternative proof for a special case of [35, Theorem 1.7]).

Theorem A. *Let $0 < p \leq 2$ and $A \in \mathcal{H}(\mathbb{D})$. If (4.1) is sufficiently small (depending on p), then all solutions of (1.2) belong to H^p.*

Proof. Note that

$$\limsup_{r\to 1^-} \sup_{a\in\mathbb{D}} \int_{\mathbb{D}} |A(rz)|^2(1-|z|^2)^2(1-|\varphi_a(z)|^2)\,dm(z) \tag{9.6}$$

is at most a constant multiple of (4.1); compare to the proof of Theorem 3. Let f be a solution of (1.2). By Theorem 4(i), we deduce

$$\begin{aligned}\|f_r\|_{H^p}^p &\lesssim \int_{\mathbb{D}} |f_r(z)|^{p-2} r^2 |f''(rz)|^2 (1-|z|^2)^3\,dm(z) + |f(0)|^p + |f'(0)|^p \\ &\lesssim \int_{\mathbb{D}} |f_r(z)|^p\,|A(rz)|^2(1-|z|^2)^3\,dm(z) + |f(0)|^p + |f'(0)|^p.\end{aligned}$$

If (9.6) is sufficiently small, then Carleson's theorem [8, Theorem 9.3] implies that $\|f_r\|_{H^p}$ is uniformly bounded for all sufficiently large $0 < r < 1$. By letting $r \to 1^-$, we obtain $f \in H^p$. □

An argument similar to the one above, taking advantage of Theorem 4(i), leads to a characterization of H^p solutions of (1.2): if $0 < p \leq 2$, f is a solution of (1.2) and $d\mu_A(z) = |A(z)|^2(1-|z|^2)^3\,dm(z)$ is a Carleson measure, then $f \in H^p$ if and only if

$$\int_{\mathbb{D}} |f(z)|^p\,d\mu_A(z) < \infty. \tag{9.7}$$

For example, if f is a normal (in the sense of Lehto and Virtanen) solution of (1.2) and μ_A is a Carleson measure, then (9.7) holds for all sufficiently small $0 < p < \infty$ by [14, Corollary 9].

Remark 5. If Question 1 had an affirmative answer, then Theorem A would admit the following immediate improvement: if $A \in \mathcal{H}(\mathbb{D})$ such that (4.1) is finite, then all solutions of (1.2) belong to $\bigcup_{0<p<\infty} H^p$.

Acknowledgements. The authors would like to thank the anonymous reviewer for valuable comments and suggestions.

References

[1] P. Ahern and J. Bruna, *Maximal and area integral characterizations of Hardy-Sobolev spaces in the unit ball of $\mathbb{C}^n$*, Rev. Mat. Iberoamericana **4** (1988), no. 1, 123–153.
[2] A. Aleman and J.A. Cima, *An integral operator on H^p and Hardy's inequality*, J. Anal. Math. **85** (2001), 157–176.
[3] A. Aleman and A. Siskakis, *Integration operators on Bergman spaces*, Indiana Univ. Math. J. **46** (1997), no. 2, 337–356.
[4] C. Chatzifountas, D. Girela and J.Á. Peláez, *Multipliers of Dirichlet subspaces of the Bloch space*, J. Operator Theory **72** (2014), no. 1, 159–191.
[5] M. Chuaqui, J. Gröhn, J. Heittokangas and J. Rättyä, *Zero separation results for solutions of second order linear differential equations*, Adv. Math. **245** (2013), 382–422.
[6] J. Cima, A. Matheson and W. Ross, *The Cauchy Transform*, Mathematical Surveys and Monographs, **125**. American Mathematical Society, Providence, RI, 2006.
[7] M.D. Contreras, J.Á. Peláez, Ch. Pommerenke and J. Rättyä, *Integral operators mapping into the space of bounded analytic functions*, J. Funct. Anal. **271** (2016), no. 10, 2899–2943.
[8] P. Duren, *Theory of H^p Spaces*, Academic Press, New York, 1970.
[9] P. Duren and A. Schuster, *Bergman Spaces*, Mathematical Surveys and Monographs, **100**, American Mathematical Society, Providence, RI, 2004.
[10] P.C. Fenton and J. Rossi, *ODEs and Wiman-Valiron theory in the unit disc*, J. Math. Anal. Appl. **367** (2010), no. 1, 137–145.

[11] J. Garnett, *Bounded Analytic Functions*, Revised first edition. Graduate Texts in Mathematics, 236. Springer, New York, 2007.
[12] D. Girela, *Analytic functions of bounded mean oscillation*, Complex function spaces (Mekrijärvi, 1999), 61–170, Univ. Joensuu Dept. Math. Rep. Ser., 4, Univ. Joensuu, Joensuu, 2001.
[13] D. Girela, J.Á. Peláez, F. Pérez-González and J. Rättyä, *Carleson measures for the Bloch space*, Integral Equations Operator Theory **61** (2008), no. 4, 511–547.
[14] J. Gröhn, A. Nicolau and J. Rättyä, *Mean growth and geometric zero distribution of solutions of linear differential equations*, to appear in J. Anal. Math. http://arxiv.org/abs/1410.2777
[15] J. Gröhn, J.Á. Peláez and J. Rättyä, *Jointly maximal products in weighted growth spaces*, Ann. Acad. Sci. Fenn. Math. **39** (2014), no. 1, 109–118.
[16] J. Gröhn and J. Rättyä, *On oscillation of solutions of linear differential equations*, J. Geom. Anal. **27** (2017), no. 1, 868–885.
[17] W. Hayman, *Multivalent Functions*, Second edition. Cambridge Tracts in Mathematics, **110**, Cambridge University Press, Cambridge, 1994.
[18] J. Heittokangas, R. Korhonen and J. Rättyä, *Growth estimates for solutions of linear complex differential equations*, Ann. Acad. Sci. Fenn. Math. **29** (2004), no. 1, 233–246.
[19] J. Heittokangas, R. Korhonen and J. Rättyä, *Linear differential equations with solutions in the Dirichlet type subspace of the Hardy space*, Nagoya Math. J. **187** (2007), 91–113.
[20] E. Hille, *Remarks on a paper by Zeev Nehari*, Bull. Amer. Math. Soc. **55** (1949), 552–553.
[21] J.-M. Huusko, T. Korhonen and A. Reijonen, *Linear differential equations with solutions in the growth space H^∞_ω*, Ann. Acad. Sci. Fenn. Math. **41** (2016), 399–416.
[22] W. Kraus, *Über den zusammenhang einiger charakteristiken eines einfach zusammenhängenden bereiches mit der kreisabbildung*, Mitt. Math. Sem. Giessen **21** (1932), 1–28.
[23] I. Laine, *Nevanlinna Theory and Complex Differential Equations*, de Gruyter Studies in Mathematics, 15. Walter de Gruyter & Co., Berlin, 1993.
[24] I. Laine, *Complex Differential Equations*, Handbook of differential equations: ordinary differential equations. Vol. IV, 269–363, Handb. Differ. Equ., Elsevier/North-Holland, Amsterdam, 2008.
[25] Z. Nehari, *The Schwarzian derivative and schlicht functions*, Bull. Amer. Math. Soc. **55** (1949), 545–551.
[26] M. Pavlović, *Green's formula and the Hardy-Stein identities*, Filomat **23** (2009), no. 3, 135–153.
[27] J.Á. Peláez, *Small weighted Bergman spaces*, Proceedings of the Summer School in Complex and Harmonic Analysis, and Related Topics, Publications of the University of Eastern Finland, Reports and Studies in Forestry and Natural Sciences (2016), No 22.
[28] J.Á. Peláez and J. Rättyä, *Weighted Bergman spaces induced by rapidly increasing weights*, Mem. Amer. Math. Soc. **227** (2014), no. 1066, vi+124 pp.
[29] J.Á. Peláez and J. Rättyä, *Embedding theorems for Bergman spaces via harmonic analysis*, Math. Ann. **362** (2015), no. 1-2, 205–239.
[30] J.Á. Peláez and J. Rättyä, *Two weight inequality for Bergman projection*, J. Math. Pures Appl. (9) **105** (2016), no. 1, 102–130.
[31] J.Á. Peláez and J. Rättyä, *Weighted Bergman projection in L^∞*, preprint.
[32] Ch. Pommerenke, *Schlichte funktionen und analytische funktionen von beschränkter mittlerer oszillation*, Comment. Math. Helv. **52** (1977), no. 4, 591–602.
[33] Ch. Pommerenke, *On the mean growth of the solutions of complex linear differential equations in the disk*, Complex Variables Theory Appl. **1** (1982/83), no. 1, 23–38.
[34] W. Rudin, *Real and Complex Analysis*, Third edition, McGraw-Hill Book Co., New York, 1987.
[35] J. Rättyä, *Linear differential equations with solutions in Hardy spaces*, Complex Var. Elliptic Equ. **52** (2007), no. 9, 785–795.
[36] B. Schwarz, *Complex nonoscillation theorems and criteria of univalence*, Trans. Amer. Math. Soc. **80** (1955), 159–186.
[37] A. Siskakis and R. Zhao, *A Volterra type operator on spaces of analytic functions*, Function spaces (Edwardsville, IL, 1998), 299–311, Contemp. Math., 232, Amer. Math. Soc., Providence, RI, 1999.
[38] W. Smith, D.M. Stolyarov and Alexander Volberg, *On Bloch approximation and the boundedness of integration operator on H^∞*, preprint. http://arxiv.org/abs/1604.05433
[39] S. Yamashita, *Schlicht holomorphic functions and the Riccati differential equation*, Math. Z. **157** (1977), no. 1, 19–22.
[40] R. Zhao, *On logarithmic Carleson measures*, Acta Sci. Math. (Szeged) **69** (2003), no. 3–4, 605–618.
[41] K. Zhu, *Operator Theory in Function Spaces*, Second edition. Mathematical Surveys and Monographs, 138. American Mathematical Society, Providence, RI, 2007.

Department of Physics and Mathematics, University of Eastern Finland,
P.O. Box 111, FI-80101 Joensuu, Finland
E-mail address: janne.grohn@uef.fi

Department of Physics and Mathematics, University of Eastern Finland, P.O. Box 111, FI-80101 Joensuu, Finland
E-mail address: juha-matti.huusko@uef.fi

Department of Physics and Mathematics, University of Eastern Finland, P.O. Box 111, FI-80101 Joensuu, Finland
E-mail address: jouni.rattya@uef.fi

Partial spectral and temporal coherence of plane-wave pulse trains in second-harmonic generation

Henri Pesonen, Juha-Matti Huusko, Xiaorun Zang, Ari T. Friberg, Jari Turunen and Tero Setälä

Institute of Photonics, University of Eastern Finland, P. O. Box 111, FI-80101 Joensuu, Finland

E-mail: henri.a.pesonen@uef.fi

Abstract. We study the spectral and temporal coherence effects in the passage of a Gaussian Schell-model (GSM) scalar, plane-wave pulse train through a slab of nonlinear optical crystal exhibiting second-harmonic generation. We show that due to the nonlinear interaction the temporal and spectral degrees of coherence of the fundamental (F) and second-harmonic (SH) pulse trains at the exit facet may deviate markedly from the GSM and the global degree of coherence of the SH wave generally decreases with increasing incident F beam intensity. In addition, we find that due to the partial coherence of the incident GSM field the transmitted SH wave may show a double-peaked intensity distribution.

1. Introduction

Coherent pulse trains of light, with each individual pulse having the same wave form, have significant applications in probing and manipulation of atoms and molecules, precision frequency metrology, telecommunications, micromachining, etc [1, 2]. However, any pulse-to-pulse variations in the pulse train render the averaged field to be partially coherent in both spectral and temporal domains [3], which necessitates a statistical analysis based on the second-order coherence theory of light. This involves concepts such as the two-frequency cross-spectral density (CSD) in the spectral domain and the two-time mutual coherence function (MCF) in the temporal domain. A great number of models [4] have been developed to describe spectrally and temporally partially coherent beams of pulsed light since the importance of the subject was recognized [5–7]. Recently, the field has expanded to cover the pulse trains especially in the contexts of supercontinuum (SC) light [8–10] and free-electron lasers [11–14].

In general, the effect of pulse train coherence of the incident (pump) beam on the various nonlinear material interactions has not been widely considered. For instance, in all studies on SC generation with photonic crystal fibers or bulk materials [15], coherent input illumination (with quantum noise) has always been taken. In this paper we will lift this assumption by letting the illuminating field be inherently partially coherent and investigate the ensuing effects on the interaction of pulse trains with nonlinear media.

A particularly important nonlinear optical effect is second-harmonic generation (SHG), with applications in, e.g., spectroscopy and remote sensing [16]. Previous studies concerning coherence and SHG relate to the SHG efficiency [17–19] and the influence of incoherence on the produced spectrum [20, 21]. Recently, the spatial coherence properties of the involved fundamental (F) and second-harmonic (SH) waves were considered in the context of stationary fields whose spectral components are necessarily uncorrelated [22].

In this work, we analyse the effect of spectral and temporal partial pulse-train coherence on SHG in a slab of optically nonlinear material. The incident field is taken to be a Gaussian Schell-model (GSM) plane-wave pulse train whose spectral (and temporal) coherence width to pulse width ratio is kept fixed and the peak intensity varied. We demonstrate that the nonlinear interaction renders the transmitted F and SH waves different from the GSM. Further, increasing the peak intensity of the incident beam decreases the overall (global) spectral and temporal degrees of coherence of the SH field and in some cases emerges a two-peaked temporal intensity profile.

The structure of this work is as follows. In Sec. 2 we introduce the concepts of optical coherence theory which are relevant for this work, while in Sec. 3 the GSM pulse trains are described. In Sec. 4 the spectral and temporal coherence properties of the F and SH pulse trains transmitted through an SHG material slab are assessed. Finally, Sec. 5 summarizes the main results. In addition, Appendix A contains a derivation of the coupled wave equations related to the SHG and describes the Runge–Kutta method for their solution.

2. Description of pulse-train coherence

We begin by recalling the relevant concepts of the scalar-field coherence theory in the spectral and temporal domains. The CSD function $W(\omega_1, \omega_2)$ measures correlations between two angular frequencies ω_1 and ω_2 and is defined as an average over scalar electric field realizations $E(\omega)$, via [23]

$$W(\omega_1, \omega_2) = \langle E^*(\omega_1) E(\omega_2) \rangle, \tag{1}$$

where the asterisk denotes complex conjugation and the angle brackets ensemble averaging. As is customary the realizations are expressed in terms of complex analytic signals. In the context of pulse trains the realizations correspond to the individual pulses and in numerical computations a finite (large) number N of them is included in the average. By setting $\omega_1 = \omega_2 = \omega$ one attains the average spectral density $S(\omega)$ which can further be used to normalize the CSD and define the complex degree of spectral coherence

$$\mu(\bar{\omega}, \Delta\omega) = \frac{W(\bar{\omega}, \Delta\omega)}{\sqrt{S(\bar{\omega} - \Delta\omega/2) S(\bar{\omega} + \Delta\omega/2)}}, \tag{2}$$

where we have used average $\bar{\omega} = (\omega_1 + \omega_2)/2$ and difference $\Delta\omega = \omega_2 - \omega_1$ coordinates. In a similar fashion, one can investigate the correlations in the temporal domain by employing the Fourier transform

$$E(t) = \int_0^\infty E(\omega) \exp(-i\omega t) \mathrm{d}\omega, \tag{3}$$

on every realization and then averaging to obtain the two-time MCF

$$\Gamma(t_1, t_2) = \langle E^*(t_1) E(t_2) \rangle. \tag{4}$$

One may normalize the MCF by the average intensity $I(t) = \Gamma(t,t)$ and get the temporal degree of coherence that reads in the average $\bar{t} = (t_1 + t_2)/2$ and difference $\Delta t = t_2 - t_1$ coordinates as

$$\gamma(\bar{t}, \Delta t) = \frac{\Gamma(\bar{t}, \Delta t)}{\sqrt{I(\bar{t} - \Delta t/2) I(\bar{t} + \Delta t/2)}}. \tag{5}$$

In many cases the degree of coherence is not constant over the pulse and a more practical way to quantify the coherence state of a pulse train is to use the overall degree of coherence. In the spectral and temporal domains the square of this quantity reads, respectively, as [7]

$$\bar{\mu}^2 = \frac{\int_{-\infty}^{\infty}\int_{0}^{\infty} |W(\bar{\omega}, \Delta\omega)|^2 \mathrm{d}\bar{\omega}\mathrm{d}\Delta\omega}{\int_{-\infty}^{\infty}\int_{0}^{\infty} S(\bar{\omega} - \Delta\omega/2) S(\bar{\omega} + \Delta\omega/2) \mathrm{d}\bar{\omega}\mathrm{d}\Delta\omega}, \tag{6}$$

$$\bar{\gamma}^2 = \frac{\int_{-\infty}^{\infty}\int_{-\infty}^{\infty} |\Gamma(\bar{t}, \Delta t)|^2 \mathrm{d}\bar{t}\mathrm{d}\Delta t}{\int_{-\infty}^{\infty}\int_{-\infty}^{\infty} I(\bar{t} - \Delta t/2) I(\bar{t} + \Delta t/2) \mathrm{d}\bar{t}\mathrm{d}\Delta t}. \tag{7}$$

These parameters obey $\bar{\mu} = \bar{\gamma}$ and $0 \le \bar{\mu}, \bar{\gamma} \le 1$.

Additional physical insight into the properties of a pulse train is obtained by investigating the coherence width to pulse width ratio. First, one may use the second moment to assess the effective spectral width, σ_s, as

$$\sigma_\mathrm{s}^2 = \frac{\int_0^\infty (\omega - \omega_0)^2 S(\omega) \mathrm{d}\omega}{\int_0^\infty S(\omega) \mathrm{d}\omega}, \tag{8}$$

$$\omega_0 = \frac{\int_0^\infty \omega S(\omega) \mathrm{d}\omega}{\int_0^\infty S(\omega) \mathrm{d}\omega}. \tag{9}$$

Second, we define an integrated measure for the degree of spectral coherence

$$\mu_\mathrm{int}(\bar{\omega}) = \int_{-\infty}^{\infty} \mu(\bar{\omega}, \Delta\omega) \mathrm{d}\Delta\omega, \tag{10}$$

and introduce the spectral density weighted effective coherence width

$$\Sigma_\mu = \frac{\int_0^\infty |\mu_\mathrm{int}(\omega)| S(\omega) \mathrm{d}\omega}{\int_0^\infty S(\omega) \mathrm{d}\omega}. \tag{11}$$

This formula emphasizes the degree of coherence at frequencies with significant spectral density. The width ratio $\Sigma_\mu/\sigma_\mathrm{s}$ then is a measure for the extent of correlations within the spectral band of the field. In a similar fashion one could define the effective pulse duration, the effective coherence time, and their ratio in the time domain. Width ratios defined in this way offer more intuitive information on the coherence characteristics of the field than the overall quantities $\bar{\mu}$ and $\bar{\gamma}$, at least in the sense that they can be seen as extensions of the width ratios into fields that are not of GSM type.

3. Gaussian Schell-model pulse trains

The GSM pulse trains constitute a special type of fields whose spectral density and degree of coherence are Gaussian functions and the latter depends only on the separation $\Delta\omega$ of the two frequencies. The CSD of a GSM plane-wave pulse train propagating along the z axis has (at $z = 0$ plane) the form [7]

$$W(\bar{\omega}, \Delta\omega) = S_0 \exp\left[-\frac{(\bar{\omega} - \omega_0)^2}{2\sigma_\mathrm{s}^2} - \frac{1}{2}\left(\frac{1}{4\sigma_\mathrm{s}^2} + \frac{1}{\sigma_\mu^2}\right)\Delta\omega^2\right], \tag{12}$$

where S_0 is the peak spectral density and σ_μ characterizes the spectral coherence width. The spectral density is given by

$$S(\omega) = S_0 \exp\left[-\frac{(\omega - \omega_0)^2}{2\sigma_\mathrm{s}^2}\right], \tag{13}$$

whereas the degree of coherence defined in Eq. (2) is

$$\mu(\Delta\omega) = \exp\left(-\frac{\Delta\omega^2}{2\sigma_\mu^2}\right). \tag{14}$$

Thus the parameters σ_s and σ_μ are the (normalized) r.m.s. widths of the spectrum and spectral coherence, respectively, associated with a pulsed GSM-type field. The width σ_s is consistent with Eq. (8) while Σ_μ of Eq. (11) satisfies $\Sigma_\mu = \sqrt{2\pi}\sigma_\mu$.

Using Eqs. (1), (3), and (4) together with Eq. (12) one finds that the MCF of a GSM pulse train is

$$\Gamma(\bar{t}, \Delta t) = I_0 \exp\left[-\frac{\bar{t}^2}{2T^2} - \frac{1}{2}\left(\frac{1}{4T^2} + \frac{1}{T_\mathrm{c}^2}\right)\Delta t^2\right] \times \exp(-i\omega_0 \Delta t), \tag{15}$$

where $I_0 = 4\pi S_0 \sigma_\mu \sigma_\mathrm{s}^2 (\sigma_\mu^2 + 4\sigma_\mathrm{s}^2)^{-1/2}$. The average intensity and the complex degree of temporal coherence are therefore given by

$$I(t) = I_0 \exp\left(-\frac{t^2}{2T^2}\right), \tag{16}$$

$$\gamma(\Delta t) = \exp\left(-\frac{\Delta t^2}{2T_\mathrm{c}^2}\right)\exp(-i\omega_0 \Delta t), \tag{17}$$

where

$$T = (\sigma_\mu^2 + 4\sigma_\mathrm{s}^2)^{1/2}/2\sigma_\mathrm{s}\sigma_\mu, \tag{18}$$

$$T_\mathrm{c} = \sigma_\mu T/\sigma_\mathrm{s}, \tag{19}$$

are the average pulse duration and the coherence time, respectively.

The CSD function in Eq. (12) admits a coherent-mode decomposition which in ω_1, ω_2 coordinates reads as

$$W(\omega_1, \omega_2) = \sum_{m=0}^{\infty} \alpha_m \psi_m^*(\omega_1) \psi_m(\omega_2), \tag{20}$$

where α_m and $\psi_m(\omega)$ are, respectively, the eigenvalues and the orthonormal eigenfunctions of a homogeneous Fredholm integral equation with the CSD as a kernel

[23]. For a GSM pulse train the eigenfunctions are Hermite-Gaussian (HG) functions [7]

$$\psi_m(\omega) = \frac{1}{\sqrt{2^m m!}} \left(\frac{2e}{\pi}\right)^{1/4} H_m\Big[\sqrt{2e}(\omega-\omega_0)\Big] \times \exp[-e(\omega-\omega_0)^2], \quad (21)$$

where $H_m(\omega)$ are Hermite polynomials, $e = (a^2 + 2ab)^{1/2}$, $a = 1/4\sigma_s^2$, and $b = 1/2\sigma_\mu^2$. The weights are given by

$$\alpha_m = S_0 \left(\frac{\pi}{a+b+e}\right)^{1/2} \left(\frac{b}{a+b+e}\right)^m. \quad (22)$$

We notice that the eigenfunctions and eigenvalues are real for a GSM beam (at the waist).

4. Effects of SHG on the coherence properties

In the following, we apply the above formalism to analyse the spectral and temporal coherence properties of the F and SH pulse trains at the output of a slab of nonlinear optical material exhibiting SHG.

4.1. Parameters of the SHG slab and the incident field

The slab has a thickness of $L = 15$ μm and an infinite transverse extent. We remark that thin films with a few micrometer (or even less than wavelength) thicknesses and supporting SHG have been employed in the context of epsilon-near-zero (ENZ) materials [24], two-dimensional atomic crystals [25], and ultrashort pulses [26]. We take the refractive index to be $n = 1.6$ for both F and SH waves. This choice together with the short propagation distance conforms to phase matching of the waves. Furthermore, the nonlinear coupling coefficient (susceptibility in contracted notation) is chosen as $d = 2.0$ pm/V. The entrance facet of the slab is set to be at the $z = 0$ plane and is illuminated by a GSM pulse train whose average spectrum, given in Eq. (13), is centered at $\omega_0 = 3.142$ rad/fs (corresponding to the wavelength of 600 nm) and has the r.m.s. width of $\sigma_s = 0.010$ rad/fs.

Throughout the work we choose the spectral coherence width in Eq. (14) as $\sigma_\mu = 0.7\sigma_s$. The pulse train therefore is spectrally rather (but not fully) coherent, and a few lowest-order modes dominate the coherent-mode decomposition of Eq. (20). More specifically, the ratios of the four lowest-order eigenvalues are given by $\alpha_1/\alpha_0 \approx 0.50$, $\alpha_2/\alpha_0 \approx 0.25$, and $\alpha_3/\alpha_0 \approx 0.13$. Hence, the energy of an individual realization is distributed essentially among a few lowest order modes. The modes with $m = 1, 2, 3$ possess amplitude peaks symmetrically around the center and this feature reflects (also after the mode-construction procedure described in Sec. 4.2) in the spectral and temporal realizations which have high-amplitude peaks (nonsymmetrically) on both sides of the center of average pulse. Further, equations (18) and (19) indicate, respectively, that the average temporal length of the pulse train is $T = 151$ fs and the coherence time is $T_c = 0.7T$. In the numerical computations that follow, all coherence widths are fixed but the peak spectral density S_0 of the incident GSM pulse train varies.

4.2. Construction and propagation of realizations

We represent the GSM field by an ensemble of $N = 500$ realizations (pulses), each of which is transmitted through a slab of nonlinear optical crystal. We checked that this number ensures the convergence of the results. The procedure for generating the ensemble is analogous to that described in [22] in the spatial domain. In short, a realization is expressed in terms of the HG modes in Eq. (21) with random coefficients and they are required to lead to the coherent-mode representation of Eq. (20). It follows that the relative weights of the HG modes constituting a realization are approximately given by $\sqrt{\alpha_m/\alpha_0}$, showing that in the arrangement considered in this work the three lowest order HG modes (with random phases) are dominant. However, we included the 50 lowest-order modes in the computations in order to ensure accuracy. We remark that several different ensembles can be generated which all represent the same incident GSM field. The various ensembles composed of different realizations then lead to different sets of the F and SH field realizations at the output which, in principle, can display distinct coherence properties for a field at the exit facet. We analysed this feature and found that the various ensembles effectively imply the same results if the number of realizations N is large and the value $N = 500$ that we use is sufficient. The analogous property but with spatial domain fields was assessed in [22].

Propagation of the F and SH pulses in a material slab is governed by the electromagnetic wave equations with nonlinear source polarizations corresponding to the SHG. These formulas are given in Eq. (A.1) of Appendix A. The nonlinear material interaction couples the two fields and induces energy transfer between them on propagation. We assume that the fields are linearly polarized in the same direction. Consequently, the F and SH fields obey the scalar wave equations, Eqs. (A.5) and (A.6), respectively, where the material interaction is specified by the susceptibility d. The coupled scalar-field wave equations are solved with the Runge–Kutta (RK) algorithm. The development of the wave equations, underlying assumptions, and the RK method are described in Appendix A.

Figure 1 exemplifies, in the case of $\sqrt{S_0} = 2.6$ GV/m, the average spectral densities (thick red and blue curves) of (a) the incident GSM pulse train and

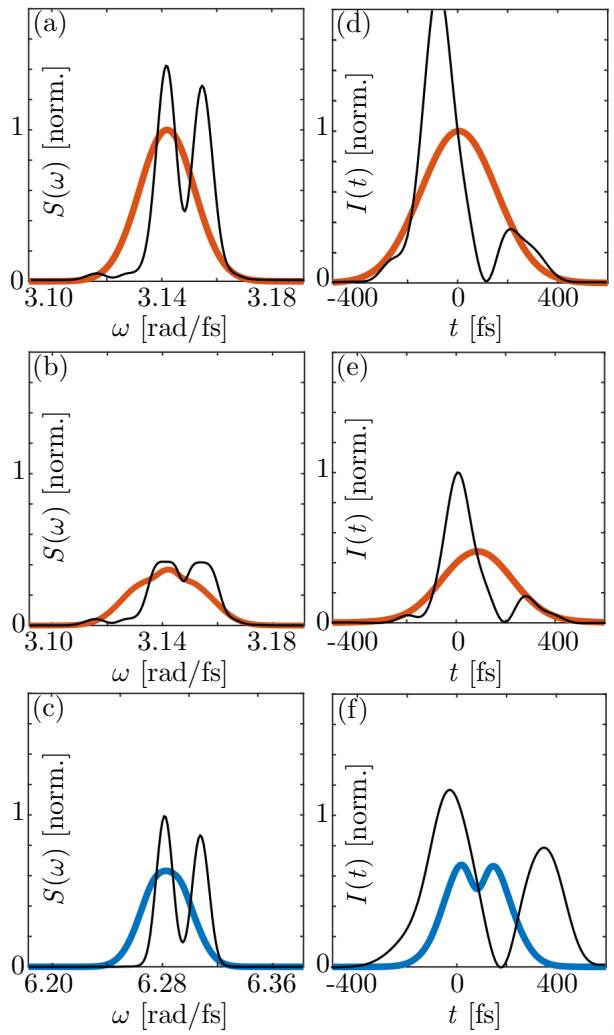

Figure 1. Illustration of typical spectral and temporal F and SH field realizations and the average spectral densities as well as intensities involved in SHG: (a,d) incident GSM pulse train, (b,e) transmitted F field, and (c,f) transmitted SH field. The thick red and blue curves refer to the average quantities whereas the thin black curves correspond to a single realization. The incident-field and slab parameters are $\sigma_s = 0.010$ rad/fs, $\sigma_\mu = 0.7\sigma_s$, $\sqrt{S_0} = 2.6$ GV/m, $L = 15$ μm, and $d = 2.0 \times 10^{-12}$ m/V. The average spectral densities and temporal intensities have been normalized by the maximum value of the corresponding incident field quantity.

the related transmitted (b) F, and (c) SH waves. The thin black curves refer to a single (typical) realization. The nonlinear crystal couples the F and SH pulses and transfers energy from the high-amplitude parts of an F realization to an SH realization. This is evident in Fig. 1 where in (c) the two amplitude peaks are located at frequencies which are two times larger than the frequencies of the two strongest F amplitude peaks in (a). As seen in (b) the amplitude of the F pulse at the corresponding locations has decreased in transmission. A similar effect takes place at the small side lobe on the left but the relative amount of transferred energy is smaller since the nonlinear material interaction is weaker at smaller field strengths. As expected, also the average spectral densities (thick curves) follow similar trends. We observe that the spectral density of the SH pulse train is centered exactly at $2\omega_0$ whereas its width is larger than that of the incident pulse train (note the different frequency scales in the figure). By using Eq. (8), the widths of the average spectra of the transmitted F and SH fields are found to be $\sigma_s = 0.011$ rad/fs and $\sigma_s = 0.016$ rad/fs, respectively. Their ratios to the spectral width of the incident field are hence 1.1 and 1.6, respectively, which indicate that both spectra are (effectively) wider than the incident one. The width values are strongly affected by the shape of the average spectrum which for both output fields deviate slightly from Gaussian showing that neither of them is a GSM pulse train.

Figures 1(d)–(f) show the temporal intensities related to the spectra in Figs. 1(a)–(c) obtained by Fourier transforming the individual realizations in terms of Eq. (3). The average intensities in (e) and (f) are centered at $t = 80$ fs corresponding to the propagation time through the slab. Part (f) demonstrates an important feature of two-peak formation in the average intensity which will be discussed in connection with Fig. 2(b).

4.3. Effect of SHG on intensity

Figure 2 depicts the distributions of the average temporal intensities of the transmitted (a) F and (b) SH pulse trains as a function of the peak amplitude $\sqrt{S_0}$ of the incident field for the same parameters as used in Fig. 1. As an example, in the case of $\sqrt{S_0} = 2.6$ GV/m (indicated by the dashed vertical line), the temporal r.m.s. widths of the incident F, transmitted F, and transmitted SH pulse trains are 151 fs, 149 fs, and 115 fs, respectively. The corresponding transmitted-to-incident pulse length ratios are 0.99 (F) and 0.76 (SH). A striking feature is seen in the shape of the SH pulse train in (b) where the intensity is double-peaked within the interval 2 GV/m $\lesssim \sqrt{S_0} \lesssim$ 15 GV/m. This effect of dual-peak formation in the SH wave train is related to partial coherence of the incident GSM pulse train. More precisely, as pointed out in Sec. 4.1, the strongest amplitude peaks of a random-shaped temporal realization of the incident partially coherent field locate on the both sides of the center of the average pulse [see Fig. 1(d)]. As the realization propagates, SHG is strongest at the peak positions resulting in an SH realization whose intensity maxima are likewise located at both sides of the center [see the black curve in Fig. 1(e)]. This feature is reflected to the average SH pulse which is

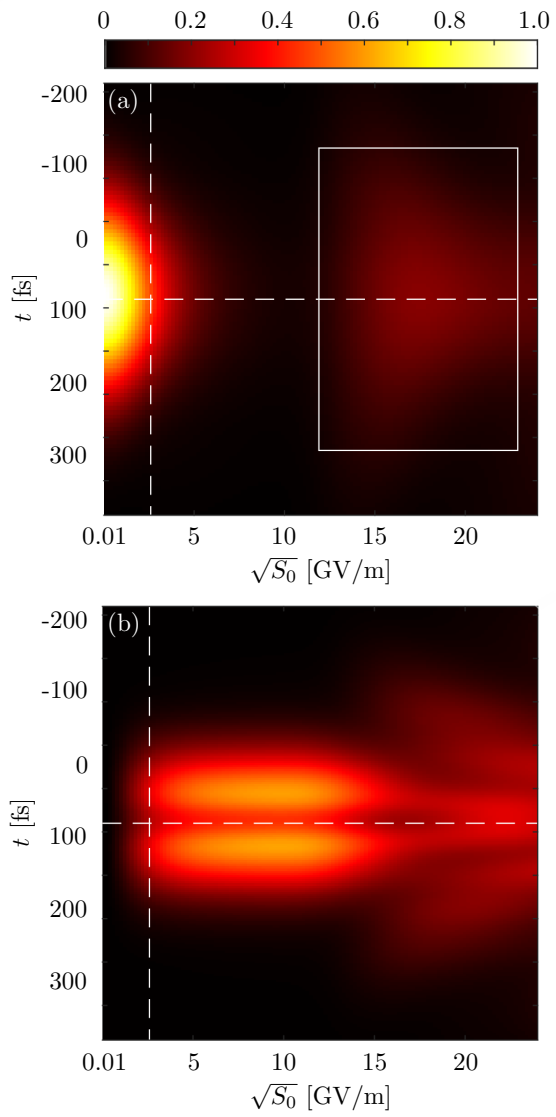

Figure 2. Average temporal intensities of the (a) F-wave and (b) SH-wave pulse trains at the output facet of the nonlinear material slab as a function of the incident GSM pulse train's peak amplitude. Otherwise the parameters of the incident field and the slab are as in Fig. 1. The dashed vertical line marks the case of $\sqrt{S_0} = 2.6$ GV/m and the distributions have been normalized by I_0. The intensity distributions are centered at $t = 80$ fs (indicated by the dashed horizontal line) which corresponds to the propagation time through the slab. The rectangle in (a) emphasizes the region where the energy transfer from the SH wave back to the F field is strongest.

two-peaked. Further, the two-peak structure of the SH beam vanishes if the incident pulse train is fully coherent (all pulses are identical and Gaussian). Thus, adjusting the partial coherence of the incident pulse train (ratio of σ_s and σ_μ) may allow to tailor the average temporal shape of the train via a nonlinear material interaction. We further observe that, above $\sqrt{S_0} \approx 15$ GV/m, a significant amount of energy transfers back to the F wave. The region where the effect is strongest is highlighted by the rectangle.

4.4. Effect of SHG on temporal and spectral coherence

Next we consider the global coherence properties of the transmitted F and SH pulse trains. The overall degrees of coherence are shown in Fig. 3(a) as a function of $\sqrt{S_0}$. For reference, we illustrate in Fig. 3(b) typical F and SH realisations for the $\sqrt{S_0}$-values of 15 and 22 GV/m in the columns from left to right, respectively. From (a) we see that the coherence of the F pulse train decreases rapidly when the peak amplitude of the incident F wave is below 10 GV/m. This behaviour is related to the decrease of the strongest peaks in the F realizations in slab transmission as explained in connection with Fig. 1. The weakening of peaks, originating from the nonlinear interaction, levels the strength differences of the amplitude maxima in the realizations and hence increases the number of dominant peaks. This is observed in the black curve of Fig. 1(b). Consequently, the transmitted F pulses with increased structural complexity represent a field with decreased overall degree of coherence. Below 10 GV/m the overall degree of coherence of the SH wave is almost constant since the generated realizations are rather simple in shape as indicated by the black curve of Fig. 1(c). When the incident peak amplitude of the F wave exceeds 10 GV/m, a significant amount of energy transfers from the SH field back to the F wave on propagation. In particular, the general behaviour of the realizations above 10 GV/m is opposite to that below this level. More precisely, the energy transfer is strongest at the locations of the highest peaks of the SH realizations levelling the strength differences of the peaks [see the lower left plot in 3(b)]. Consequently, the degree of coherence decreases rapidly within 10 GV/m $\lesssim \sqrt{S_0} \lesssim$ 17 GV/m. We verified numerically that in this interval the F realizations take simpler forms, with essentially a single dominant peak [see the upper left figure in 3(b)], and hence the degree of coherence increases. Above 17 GV/m the energy transfer process between the F and SH waves is again reversed. In addition, the level of coherence decreases in both waves as indicated by the increased number of peaks in the realizations of the right column of (b). We remark that the above effects were found for a chosen L-value and with thicker slabs the effects would occur at lower incident intensities.

Besides the overall degree of coherence, an illustrative measure for the range of correlations (coherence) within the pulse train is the coherence width to pulse width ratio, Σ_μ/σ_s, which can be obtained from Eqs. (8) and (11). This ratio for the transmitted F and SH pulses is shown in Fig. 3(b) with red and blue curves, respectively. The main features

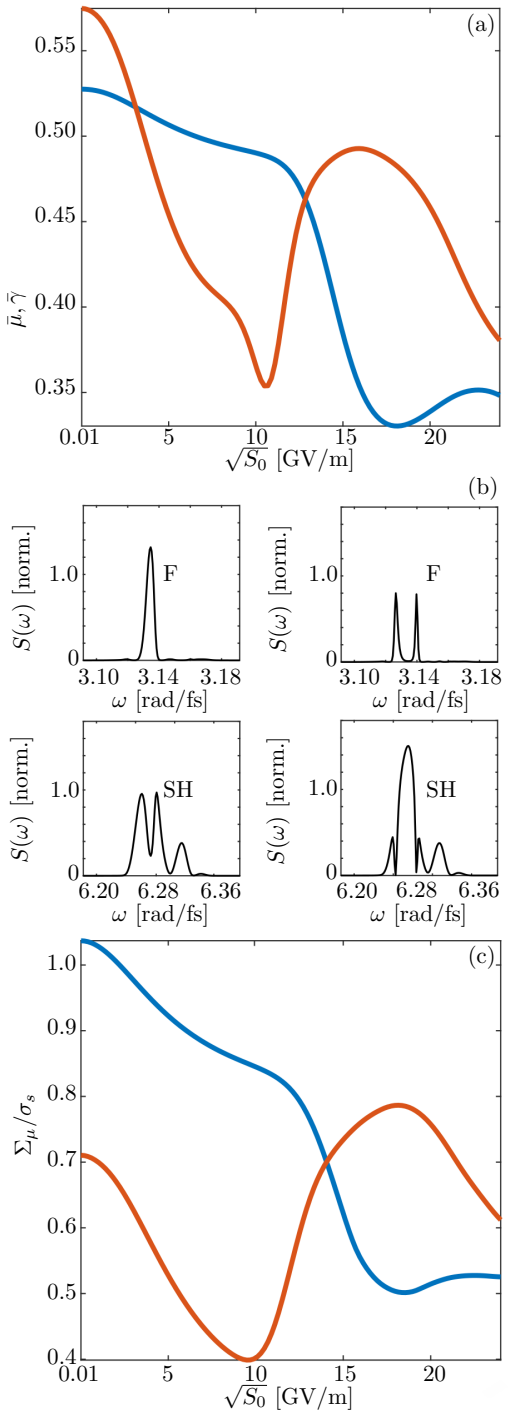

Figure 3. Illustration of the coherence properties related to the transmitted F (red curves) and SH (blue curves) pulse trains as a function of the incident GSM pulse train's peak amplitude. (a) The overall temporal and spectral degrees of coherence ($\bar{\mu} = \bar{\gamma}$), (b) the spectra of typical F and SH realizations for $\sqrt{S_0} = (15, 22)$ GV/m corresponding to columns from left to right, and (c) coherence width to pulse width ratio. Apart from varying S_0 the parameters of the incident field and the slab are as in Fig. 1. The curves in (b) have been normalized by S_0.

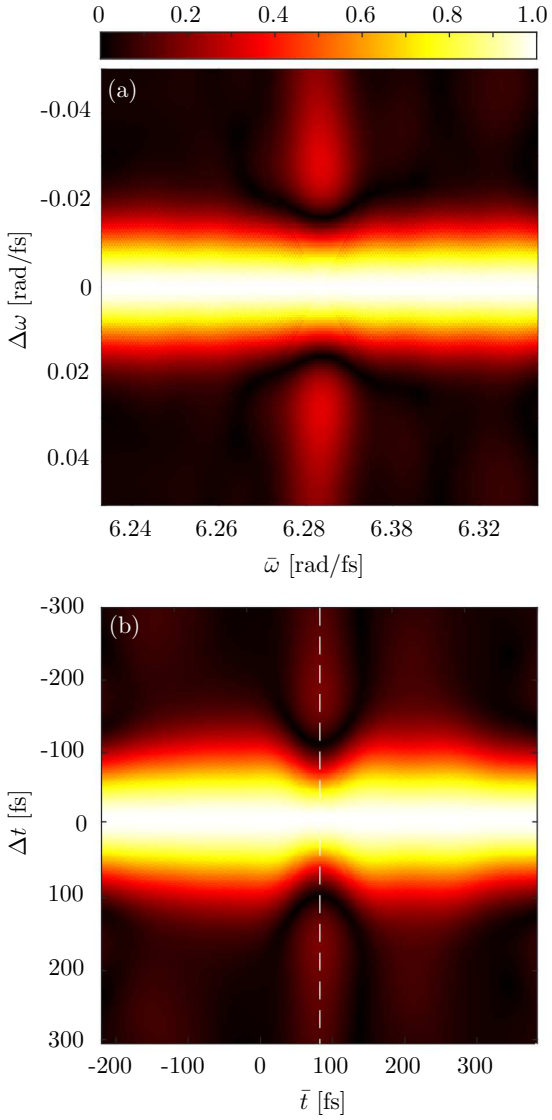

Figure 4. Distributions of the magnitudes of the degrees of coherence in (a) the spectral domain and (b) the temporal domain, of the transmitted SH field. The various geometry parameters are as in Fig. 1. The dashed line marks the location $\bar{t} = 80$ fs which corresponds to the propagation time through the slab. In the center region the spectral and temporal coherences are modulated in the $\Delta\omega$ and Δt directions, respectively, with minima at $\Delta\omega = \pm 0.016$ rad/s and $\Delta t = \pm 102$ fs.

are the same as in (a). At this stage we summarize by noting that, within the considered amplitude range, the global coherence of the SH wave generally decreases at the exit facet whereas that of the F field oscillates with increasing incident field intensity.

Figures 4(a) and 4(b) show the spectral and temporal degrees of coherence, respectively, for the transmitted SH pulse train at $\sqrt{S_0} = 2.6$ GV/m. In the vicinity of $\bar{\omega} = 2\omega_0 = 6.284$ rad/fs the SH field deviates from the GSM type, for which the

magnitude of the degree of coherence would be a horizontal bar in the average and difference frequency coordinates. At $\bar{\omega} = 2\omega_0$ the degree exhibits a modulation in the $\Delta\omega$ direction with minima at $\Delta\omega = \pm 0.016$ rad/s. A similar modulation effect as shown here for the SH field exists also in the transmitted F pulse train. In general, Fig. 4(a) demonstrates that for the transmitted SH field the spectral correlations around the center frequency extend farther than in the edge regions of the spectrum.

Also the temporal degree of coherence exhibits modulation as seen in Fig. 4(b). More precisely, the degree is modulated in the Δt direction close to $\bar{t} = 80$ fs (dashed line), which corresponds to the time of propagation through the slab, and assumes minimum value at $\Delta t = \pm 102$ fs. An essential feature is that the temporal degree of coherence deviates from the GSM form, for which the distribution would be horizontal bar whose width is specified by the temporal coherence width. In particular, close to $\bar{t} = 80$ fs, the temporal correlations extend farther that in the tail parts.

Figure 4 illustrates the particular case of $\sqrt{S_0} = 2.6$ GV/m, for which the intensity distribution exhibits the double-peak structure shown in Fig. 2. If the incident amplitude $\sqrt{S_0}$ is increased the modulation of the spectral and temporal degrees of coherence in Fig. 4 vanishes and the degrees become narrower around $\bar{\omega} = 2\omega_0$ and $\bar{t} = 80$ fs, respectively. This decreases the SH overall degrees of coherence in the two domains at high $\sqrt{S_0}$ values as observed in Fig. 3 above 10 GV/m.

5. Conclusions

As a summary, we considered an incident scalar, GSM plane-wave pulse train and evaluated the spectral and temporal coherence properties of the F and SH waves at the output facet of an optical crystal exhibiting SHG when the GSM peak amplitude was varied. Throughout the work the spectral (and temporal) coherence width to pulse width ratio of the incoming field was fixed at 0.7 indicating the we considered a rather coherent pulse train. We found that both transmitted beams, in general, may deviate essentially from the GSM as the correlation lengths within the pulse spectrum and temporal intensity vary. Further, the global degree of coherence of the F field at the output oscillates while that of the SH wave decreases with increasing incident intensity. We also found that for some input beam intensities partial coherence of the incident field induces a two-peak temporal intensity distribution for the SH field. The results of this work demonstrate that when SHG with a partially coherent pulse train is employed to produce light at frequencies which are not directly available or where efficient detectors exists the coherence properties may have a significant effect on the characteristics of the SH field.

Acknowledgements

Academy of Finland (projects 308393 and 310511). The work is part of the Academy of Finland Flagship Programme, Photonics Research and Innovation (PREIN, 320166).

Appendix A. Coupled wave equations for the F and SH waves

We first derive the coupled wave equations for the fundamental (F) and the second-harmonic (SH) plane-wave pulse fields that govern their propagation in a material exhibiting second-harmonic generation. Along the derivation we highlight the underlying assumptions. At the end, we describe the Runge–Kutta (RK) method that was employed to solve the two equations.

As the F and SH light fields propagate their amplitudes are coupled by the induced nonlinear polarization. In general, the fields require electromagnetic treatment and hence we denote the electric fields of the F and SH spectral pulses by $\mathbf{E}_1(\mathbf{r},\omega_1)$ and $\mathbf{E}_2(\mathbf{r},\omega_2)$, respectively. Notice that the angular frequencies ω_1 and ω_2 refer to the F and SH waves and they should not be confused with the frequency arguments of the CSD in the main text. Both fields are plane-wave pulses and we set them to propagate along the z axis. We assume that the medium is homogeneous, nonmagnetic, contains no free charges and currents, and its linear response is local and isotropic with negligible dispersion. The behaviours of the two fields are in the spectral domain governed by the inhomogeneous wave equations [16]

$$\nabla\times\nabla\times\mathbf{E}_m(\mathbf{r},\omega_m) - k_m^2\mathbf{E}_m(\mathbf{r},\omega_m) = \mu_0\omega_m^2\mathbf{P}_m^{(\mathrm{NL})}(\mathbf{r},\omega_m), \quad m=(1,2), \quad \text{(A.1)}$$

where $\mathbf{r}$ refers to a point in space, $k_m = n\omega_m/c$ is the wave number at angular frequency ω_m with c being the vacuum speed of light, and μ_0 is the vacuum permeability. In addition, n is the refractive index which is set independent of frequency due to weak dispersion. Moreover, $\mathbf{P}_m^{(\mathrm{NL})}(\mathbf{r},\omega_m)$ is the nonlinear (source) polarization at frequency ω_m, whose $i=(x,y)$ component generally reads as

$$P_{mi}^{(\mathrm{NL})}(\mathbf{r},\omega_m) = \epsilon_0\sum_{jk}\chi_{ijk}^{(2)}(\omega_m,\omega_a,\omega_b)E_j(\mathbf{r},\omega_a)E_k(\mathbf{r},\omega_b), \quad \text{(A.2)}$$

where $\chi_{ijk}^{(2)}(\omega_m,\omega_a,\omega_b)$ is the second-order nonlinear susceptibility with $\omega_m = \omega_a + \omega_b$. The quantities

$E_j(\mathbf{r},\omega_a)$ and $E_k(\mathbf{r},\omega_b)$, with $(j,k)=(x,y)$, represent the Cartesian field components at frequencies ω_a and ω_b. For the SH field $\omega_m=\omega_2$, $\omega_a=\omega_b=\omega_1$ while for the F wave $\omega_m=\omega_1$, $\omega_a=\omega_2$, and $\omega_b=-\omega_1$ hold.

Next we take both fields to be linearly polarized in the x direction reducing the problem to a scalar-field case conforming to the theory of the main text. The source polarizations for the F and SH fields in Eq. (A.2) take the respective forms

$$P_1^{(\mathrm{NL})}(\mathbf{r},\omega_1) = 2\epsilon_0\chi^{(2)}_{xxx}(\omega_1,\omega_2,-\omega_1)E_x(\mathbf{r},\omega_2)E_x^*(\mathbf{r},\omega_1), \quad (A.3)$$

$$P_2^{(\mathrm{NL})}(\mathbf{r},\omega_2) = \epsilon_0\chi^{(2)}_{xxx}(\omega_2,\omega_1,\omega_1)E_x^2(\mathbf{r},\omega_1). \quad (A.4)$$

In Eq. (A.3) we used the intrinsic permutation symmetry of the susceptibility and the property $E_x(\mathbf{r},-\omega_1)=E_x^*(\mathbf{r},\omega_1)$. Assuming the Kleinmann symmetry condition and invoking the contracted notation $\chi^{(2)}_{xxx}(\omega_2,\omega_1,\omega_1)=2d_{11}=2d$, enables to develop the two wave equations in Eq. (A.1) into the form

$$\frac{\partial^2 E_1(z,\omega_1)}{\partial z^2}+k_1^2E_1(z,\omega_1) = -4\frac{\omega_1^2 d}{c^2}E_1^*(z,\omega_1)E_2(z,\omega_2), \quad (A.5)$$

$$\frac{\partial^2 E_2(z,\omega_2)}{\partial z^2}+k_2^2E_2(z,\omega_2) = -2\frac{\omega_2^2 d}{c^2}E_1^2(z,\omega_1). \quad (A.6)$$

Here we also used the fact that $\nabla\cdot\mathbf{E}_m(\mathbf{r},\omega_m)=0$ holds for both $m=(1,2)$ since the fields are plane-wave pulses. In addition, we employed the invariance of the fields in the transverse direction and some basic properties of the nonlinear susceptibility. Notice that the reduction to the scalar-field case requires that the medium is such that d_{11} is the only significant element of the material's d matrix.

The numerical procedure of the F and SH wave propagation is based on the RK method [27] and is as follows. We first write $E_m(z,\omega_m)=A_m(z,\omega_m)\exp(ik_mz)$, $m=(1,2)$, and assume that the waves are phase matched obeying $\Delta k=k_2-2k_1=0$. Equations (A.5) and (A.6) thus transform into

$$\frac{\partial^2 A_1(z,\omega_1)}{\partial z^2}+2ik_1\frac{\partial A_1(z,\omega_1)}{\partial z} = -4\frac{\omega_1^2 d}{c^2}A_1^*(z,\omega_1)A_2(z,\omega_2), \quad (A.7)$$

$$\frac{\partial^2 A_2(z,\omega_2)}{\partial z^2}+2ik_2\frac{\partial A_2(z,\omega_2)}{\partial z} = -2\frac{\omega_2^2 d}{c^2}A_1^2(z,\omega_1). \quad (A.8)$$

Next we introduce a new variable $A'_m(z,\omega_m)=\partial A_m(z,\omega_m)/\partial z$ which allows us to split the above pair of equations as

$$\frac{\partial A_1(z,\omega_1)}{\partial z}=A'_1(z,\omega_1), \quad (A.9)$$

$$\frac{\partial A'_1(z,\omega_1)}{\partial z} = -2ik_1A'_1(z,\omega_1) - 4\frac{\omega_1^2 d}{c^2}A_1^*(z,\omega_1)A_2(z,\omega_2), \quad (A.10)$$

$$\frac{\partial A_2(z,\omega_2)}{\partial z}=A'_2(z,\omega_2), \quad (A.11)$$

$$\frac{\partial A'_2(z,\omega_2)}{\partial z} = -2ik_2A'_2(z,\omega_2)-2\frac{\omega_2^2 d}{c^2}A_1^2(z,\omega_1). \quad (A.12)$$

This set of equations can be integrated with respect to z in terms of the RK algorithm.

The accuracy of the RK method was verified by COMSOL simulations which implied identical results. We used a two-dimensional model in the COMSOL analysis with the mesh element size down to $\lambda_1/50$. In brief, Eq. (A.1) at F and SH frequencies are coupled and solved under two Electromagnetic Waves, Frequency Domain (ewfd) interfaces [28]. Equations (A.3) and (A.4), respectively, are used to set the Polarization node under each ewfd interface for coupling the F and SH light fields.

We also point out that the commonly used slowly-varying envelope approximation (SVEA) [16], which we also tried in analogy with the spatial-domain analysis in [22], failed to predict the transfer of power back to the F wave after certain pump power levels ($\sqrt{S_0}$ above 15 GV/m, see Fig. 2). We therefore resorted to rigorous solutions of Maxwell's equations by the RK algorithm.

References

[1] Saleh B E A and Teich M C 2007 *Fundamentals of Photonics* 2nd edn (Hoboken: Wiley)

[2] Trebino R 2000 *Frequency-Resolved Optical Gating: The Measurement of Ultrashort Laser Pulses* (Amsterdam: Kluwer Academic)

[3] Walmsley I A and Dorrer C 2009 Characterization of ultrashort electromagnetic pulses *Adv. Opt. Photon.* **1** 308–437

[4] Cai Y, Chen Y and Wang F 2014 Generation and propagation of partially coherent beams with nonconventional correlation functions: a review [Invited] *J. Opt. Soc. Am. A* **31** 2083–96

[5] Christov I P 1986 Propagation of partially coherent light pulses *Opt. Acta* **33** 63–72

[6] Pääkkönen P, Turunen J, Vahimaa P, Friberg A T and Wyrowski F 2002 Partially coherent Gaussian pulses *Opt. Commun.* **204** 53–8

[7] Lajunen H, Tervo J and Vahimaa P 2004 Overall coherence and coherent-mode expansion of spectrally partially coherent plane-wave pulses *J. Opt. Soc. Am. A* **21** 2117–23

[8] Genty G, Surakka M, Turunen J and Friberg A T 2010 Second-order coherence of supercontinuum light *Opt. Lett.* **35** 3057–9

[9] Genty G, Surakka M, Turunen J and Friberg A T 2011 Complete characterization of supercontinuum coherence *J. Opt. Soc. Am. B* **28** 2301–9

[10] Närhi M, Turunen J, Friberg A T and Genty G 2016 Experimental measurement of the second-order coherence of supercontinuum *Phys. Rev. Lett.* **116** 243901

[11] Mitzner R *et al.* 2008 Spatio-temporal coherence of free electron laser pulses in the soft X-ray regime 2008 *Opt. Express* **16** 19909–19

[12] Roling S, Siemer B, Wöstmann M, Zacharias H, Mitzner R, Singer A, Tiedtke K and Vartanyants I A 2011 Temporal and spatial coherence properties of free-electron laser pulses in the extreme ultraviolet region *Phys. Rev. Special Topics – Accel. Beams* **14** 080701

[13] Vartanyants I A *et al.* 2001 Coherence properties of individual femtosecond pulses of an X-ray free-electron laser *Phys. Rev. Lett.* **107** 144801

[14] Ahad L, Vartiainen I, Setälä T, Friberg A T, David C, Makita M and Turunen J 2016 On spectral and temporal coherence of X-ray free-electron laser beams *Opt. Express* **24** 13081–90

[15] Genty G, Friberg A T and Turunen J 2016 Chap 2 *Coherence of supercontinuum light* in *Progress in Optics* vol 61, ed T Visser (Amsterdam: Elsevier) pp 71–111

[16] Boyd R W 2008 *Nonlinear Optics* 3rd edn (New York: Academic Press).

[17] Zubairy M S and McIver J K 1987 Second-harmonic generation by a partially coherent beam *Phys. Rev. A* **36** 202–6

[18] Cai Y and Peschel U 2007 Second-harmonic generation by an astigmatic partially coherent beam *Opt. Express* **15** 15480–92

[19] Ji L *et al.* 2019 High-efficiency second-harmonic generation of low-temporal-coherent light pulse *Opt. Lett.* **44** 4359–62

[20] Pyragaite V, Stabinis A and Piskarskas A 2012 Frequency spectrum of second-harmonic radiation exited by a Gaussian Schell-model beam *Phys. Rev. A* **86** 033812

[21] Stanislovaitis P, Narmontas A, Pyragaite V and Smilgevičius V 2014 Generation of a second-harmonic beam from incoherent conical beams *Phys. Rev. A* **89** 043821

[22] Pesonen H, Halder A, Huusko J–M, Friberg A T, Setälä T and Turunen J 2021 Spatial coherence effects in second-harmonic generation of scalar light fields *J. Opt.* **23** 035501

[23] Mandel L and Wolf E 1995 *Optical Coherence and Quantum Optics* (Cambridge: Cambridge University Press)

[24] Passler N C, Razdolski I, Katzer D S, Storm D F, Caldwell J D, Wolf M and Paarmann A 2019 Second harmonic generation from phononic epsilon-near-zero Berreman modes in ultrathin polar crystal films *ACS Photon.* **6** 1365–71

[25] Zhao M, Ye Z, Suzuki R, Ye Y, Zhu H, Xiao J, Wang Y, Iwasa Y and Zhang X 2016 Atomically phase-matched second-harmonic generation in a 2D crystal *Light: Sci. Appl.* **5** e16131

[26] Sidick E, Knoesen A and Dienes A 1995 Ultrashort-pulse second-harmonic generation. I. Transform-limited fundamental pulses *J. Opt. Soc. Am. B* **12** 1704–12

[27] Butcher J C 2016 *Numerical Methods for Ordinary Differential Equations* 3rd edn (Hoboken: Wiley)

[28] Wave Optics Module User's Guide, pp. 70-113. COMSOL Multiphysics v. 5.5. COMSOL AB, Stockholm, Sweden, 2019.

Spatial coherence effects in second-harmonic generation of scalar light fields

Henri Pesonen[1], Atri Halder[1], Juha-Matti Huusko[2], Ari T. Friberg[1], Tero Setälä[1] and Jari Turunen[1]

[1]Institute of Photonics, University of Eastern Finland, P. O. Box 111, FI-80101 Joensuu, Finland
[2]Department of Physics and Mathematics, University of Eastern Finland, P. O. Box 111, FI-80101 Joensuu, Finland

E-mail: henri.a.pesonen@uef.fi

June 2020

Abstract. We consider the spectral spatial coherence characteristics of scalar light fields in second-harmonic generation in an optically nonlinear medium. Specifically, we take the fundamental-frequency (incident) field to be a Gaussian Schell-model (GSM) beam with variable peak spectral density and different coherence properties. We show that with increasing intensity the overall degree of coherence of both the fundamental and the second-harmonic field in general decreases on passage through the nonlinear medium. In addition, the spectral density distributions and the two-point degree of coherence may, for both beams, deviate significantly from those of the GSM, especially at high intensities. Propagation in nonlinear medium is numerically analyzed with the Runge–Kutta and the beam-propagation method of which the latter is found to be considerable faster. The results of this work provide means to synthesize, via nonlinear material interaction, random optical beams with desired coherence characteristics.

1. Introduction

Optical coherence [1, 2] and nonlinear optics [3, 4] are central research areas of modern optics. Both topics are extensive but the influence of partial optical coherence (temporal, spatial, or spectral) in nonlinear light-matter interactions has been analyzed only in a few specific cases. For example, in the context of second-harmonic generation (SHG) the conversion efficiency with an incident spatially [5] and temporally [6] partially coherent beam as well as with astigmatic beams [7] has been considered. Further, the spectral properties of the second-harmonic field induced by a Gaussian Schell-model (GSM) beam [8] and an incoherent conical beam [9] have been investigated. Other researches cover, e.g., the effect of an incoherent pump beam in parametric amplification [10], spatial coherence of local second-harmonic fields at rough metal surfaces [11], pulse propagation in Kerr medium [12], and supercontinuum coherence [13–15].

In this work, we assess, within the scalar-field formalism, the coherence properties of the second-harmonic field produced by a stationary GSM beam in a nonlinear optical material. We use the depleted (incident) beam model that takes into account the effect of the nonlinear interaction on the incident fundamental-frequency GSM beam. Hence, besides the second-harmonic field, we also consider the coherence changes in the fundamental-frequency beam. The random GSM beam in front of the crystal is represented by constructing an ensemble of monochromatic (random-shaped) realizations. Each realization is then propagated through the nonlinear crystal one at a time using the Runge–Kutta (RK) algorithm and the beam-propagation (BP) method tailored for the present context. Both techniques provide highly similar results, but the latter technique is observed to be two orders of magnitude faster. In general, the degrees of coherence of both the fundamental and the second-harmonic wave are found to decrease on passage through the crystal. The origin of this effect is the second-harmonic creation at the strongest peaks of the fundamental-wave realizations which increases the structural complexity in the realizations of both fields. The effect is stronger for higher incident-field peak intensities leading to fundamental and second-harmonic fields whose coherence properties may deviate significantly from the GSM. Nonlinear material response can therefore be used to control and tailor the coherence properties of random beams.

This work is organized as follows. In Sec. 2 the GSM beam and its propagation in a nonlinear medium supporting SHG are described. Section 3 is devoted to the numerical analysis of the coherence effects taking place in SHG and Sec. 4 is a summary of the main results. Several theoretical aspects have been relegated to Appendices A-D. In A the construction of an ensemble representing a GSM beam is described. In B and C the RK and BP propagation methods, respectively, are outlined and D evaluates the sufficient number of realizations.

2. Second-harmonic generation with a Gaussian Schell-model beam

In this section we introduce the relevant concepts concerning the GSM beams and their propagation in a nonlinear medium exhibiting SHG.

2.1. Gaussian Schell-model beams

The spatial coherence properties of a stationary scalar light beam at points x_1 and x_2 in a plane $z = z_0$ and at frequency ω are described by the cross-spectral density (CSD) function. The CSD can be defined as [1]

$$W(x_1, x_2, z_0; \omega) = \langle E^*(x_1, z_0; \omega) E(x_2, z_0; \omega) \rangle, \qquad (1)$$

where the asterisk denotes complex conjugation and the angular brackets refer to ensemble averaging. In addition, $E(x, z_0; \omega)$ is a monochromatic field realization representing a random electric field which in this work is taken to be linearly polarized. Also the field generated in nonlinear interaction is similarly linearly polarized allowing a scalar treatment of all fields. In this section, we drop the explicit frequency and z dependencies for notational simplicity and assume that the formulas are given at the entrance facet of a nonlinear crystal. By setting $x_1 = x_2 = x$ we obtain the (average) spectral density of the field as $S(x) = W(x, x)$. The normalized CSD, namely the complex (spectral) degree of spatial coherence, reads

$$\mu(x_1, x_2) = \frac{W(x_1, x_2)}{\sqrt{S(x_1) S(x_2)}}. \qquad (2)$$

It is known that the CSD admits the coherent-mode representation [1, 2], i.e., an expansion in terms of the

mutually uncorrelated, spatially fully coherent modes. This is explicitly given by

$$W(x_1, x_2) = \sum_{m=0}^{\infty} \alpha_m \psi_m^*(x_1)\psi_m(x_2), \tag{3}$$

where the weights α_m are real and nonnegative and the mode functions $\psi_m(x)$ are orthonormal in the considered region. The eigenvalues and eigenfunctions are solutions of a Fredhold integral equation [1]. For a GSM beam the mode functions are of Hermite-Gaussian (HG) form, written as [1,16]

$$\psi_m(x) = \frac{(2/\pi)^{1/4}}{\sqrt{2^m m! w_0}} H_m\left(\frac{\sqrt{2}x}{w_0}\right) \exp\left(-\frac{x^2}{w_0^2}\right), \tag{4}$$

while the modal weights are

$$\alpha_m = S_0 \sqrt{\frac{2\pi}{\beta}} \frac{w_0}{1+1/\beta} \left(\frac{1-\beta}{1+\beta}\right)^m. \tag{5}$$

Above, S_0 is the (spatial) peak spectral density, w_0 represents the mode width, and $H_m(x)$ is a Hermite polynomial. Parameter β is a real constant ranging between $0 \leq \beta \leq 1$ and it connects the width w of the GSM beam and w_0 as $w = w_0/\sqrt{\beta}$.

The full CSD of a GSM beam can be expressed as

$$W(x_1, x_2) = S_0 \exp\left(-\frac{1+\beta^2}{2\beta}\frac{x_1^2 + x_2^2}{w_0^2}\right) \times \exp\left(\frac{1-\beta^2}{\beta}\frac{x_1 x_2}{w_0^2}\right), \tag{6}$$

and the related spectral density is

$$S(x) = S_0 \exp\left(-\frac{2x^2}{w^2}\right). \tag{7}$$

These enable us to write the complex degree of coherence of Eq. (2) in the form

$$\mu(x_1, x_2) = \exp\left[-\frac{(x_2 - x_1)^2}{2\sigma^2}\right], \tag{8}$$

where $\sigma = \sqrt{\beta/(1-\beta)}w_0$ describes the coherence width of the GSM beam. We further introduce the overall (effective) degree of coherence [17,18]

$$\bar{\mu}^2 = \frac{\int_{-\infty}^{\infty}\int_{-\infty}^{\infty} |W(x_1, x_2)|^2 \mathrm{d}x_1 \mathrm{d}x_2}{\int_{-\infty}^{\infty}\int_{-\infty}^{\infty} S(x_1)S(x_2)\mathrm{d}x_1\mathrm{d}x_2}, \tag{9}$$

which characterizes the intensity-weighted degree of spatial coherence. For a GSM beam, $\bar{\mu} = \sqrt{\beta}$ holds.

2.2. Propagation in nonlinear medium

In this work, a GSM beam is propagated through a nonlinear medium one realization $E(x, z; \omega)$ at a time. The construction of a statistical ensemble of realizations that represents a GSM beam is described in Appendix A. We assume that the medium is nonmagnetic, source free, and its (dispersive) linear response is isotropic. The nonlinear response of the medium is taken local and its strength is expressed by the nonlinear susceptibility d (in contracted notation) under the Kleinman symmetry conditions. We from now on refer to field $E(x, z; \omega)$ as the fundamental (F) wave and invoke the notation $E_1(x, z) = E(x, z; \omega_1)$. The second-harmonic (SH) wave at frequency $\omega_2 = 2\omega_1$ generated in the medium is denoted by $E_2(x, z)$. The two waves are coupled in propagation and obey [3]

$$\nabla^2 E_1(x, z) + k_1^2 E_1(x, z) = -4\frac{d\omega_1^2}{c^2} E_1^*(x, z) E_2(x, z), \tag{10}$$

$$\nabla^2 E_2(x, z) + k_2^2 E_2(x, z) = -2\frac{d\omega_2^2}{c^2} E_1^2(x, z), \tag{11}$$

where $k_i = n(\omega_i)\omega_i/c$ with $n(\omega_i)$ being the refractive index, $i \in (1, 2)$, and c is the vacuum speed of light.

The above coupled equations are numerically solved by employing the RK method outlined in Appendix B and the BP method described in Appendix C. We compared these methods in the context of field propagation in a nonlinear medium. The implementation is with Matlab and the two methods rely on the available RK and Fast Fourier Transform (FFT) algorithms. As an example, with 600 and 20000 sampling points in the transverse and longitudinal directions, respectively, the calculation times were 165.5 s with the RK and 0.7 s with the BP method. Thus, the BP method can here be regarded as two orders of magnitude faster than the RK technique. As an example, in Appendix C the output spectral density distributions of the F and SH waves computed with the two methods are considered in a specific case. It is verified that with high accuracy the methods lead to identical results.

We notice that different ensembles can produce different SH-field coherence properties since the input F-field realizations themselves affect the generated SH field realizations via nonlinear interaction. We assessed this possible effect by calculating the coherence properties of the F and SH fields at the output of the nonlinear crystal for several ensembles of realizations. It turned out that for sufficiently large ensembles the SH-wave coherence properties were effectively the same for all sets. The same holds for the F waves. These are important justifications for the validity of the method. The influence of the number of members in an ensemble is considered in Appendix D. It is found that the coherence properties reach convergence (are essentially unaltered if more realizations are included) when the number of realizations exceeds about three hundred.

3. Numerical results

In this section we evaluate numerically the spatial coherence properties of the F and SH beams propagating in a nonlinear medium. We employ the

BP method for field propagation as it was confirmed to be significantly faster than the RK technique. The incident (F) field is a linearly (fully) polarized GSM beam at frequency ω_1. In the entrance facet of the crystal (chosen to be at $z = 0$) the field is represented by a set of realizations $\{E_{1n}(x, 0)\}$ whose construction is explained in Appendix A. Averaging over all realizations leads to the CSD of Eq. (6) as well as to the Gaussian spectral density of Eq. (7) and the degree of coherence described by Eq. (8). The width of the incident beam is in all considered cases fixed at $w = w_0/\sqrt{\beta} = 40\lambda_1$ with the (vacuum) wavelength of the F wave being $\lambda_1 = 0.8$ μm. The effective degree of coherence of the incident beam is varied by taking $\beta \in \{0.3, 0.5, 0.7, 0.85, 0.97\}$, where the extremes correspond to a weakly and highly coherent beams, respectively. We do not consider lower β values since the beam width is $40\lambda_1$ and the transverse coherence length is in practise at least a few wavelengths. For each β value, we consider the spectral densities specified by $\sqrt{S_0} \in [0.001$ GV/m, 0.8 GV/m$]$. This accordingly affects the amplitudes of the individual realizations in the ensemble and stronger amplitudes are expected to imply more notable nonlinear effects. Furthermore, we choose the length L of the crystal as $L = 0.5$ mm and take the medium to be such that the F and SH waves have the same linear polarization state which is preserved on propagation. Hence, the nonlinear susceptibility has only one nonzero element whose value is taken as $d = 2.0 \times 10^{-12}$ m/V. All the parameters are chosen such that measurements are possible, at least in principle, with a picosecond pulse laser, for instance. We remark that the strength of the SH wave can be enhanced by increasing either the incident spectral density or the crystal length [19]. However, in this work the crystal length is kept fixed.

In the following we consider two cases. First, the refractive index of the crystal is the same at both frequencies, $n(\omega_1) = n(\omega_2) = 1.66$. Second, the indices are different, $n(\omega_1) = 1.660$, $n(\omega_2) = 1.661$. We refer to these situations as the 'phase-matched case' and the 'phase-mismatched case', respectively. We ignore the back reflections at the output facet as the related reflectance for the slab with chosen indices (surrounded by air) is a few percent at normal incidence.

3.1. Phase-matched case

Taking the refractive indices the same at the two frequencies, we calculate the squared overall degree of coherence for both the F and SH beams as a function of the incident beam's $\sqrt{S_0}$, which is a measure for the average peak amplitude. The computations are carried out for several β values and the results are shown in Fig. 1. The pink, yellow, blue, green, and orange curves refer to the β values of 0.3, 0.5, 0.7, 0.85, and 0.97, respectively. In addition, the solid lines indicate the F waves whereas the dashed lines denote the SH beam. We note that with small incident-field amplitudes, the degree of coherence of the F field does not change upon passage. This is explained by the facts that the propagation distance is short and the low amplitude does not induce significant SHG.

We further see from Fig. 1 that when $\sqrt{S_0}$ is increased, the effective degree of coherence of the F beam reduces rapidly for all β. At the same time, the SH beam's $\bar{\mu}$ remains nearly constant. Consequently, for all β values, the SH beam's degree of coherence at some point becomes larger than that of the F beam. This subsequently holds within a certain amplitude range which is the wider the higher is the incident F-wave β value. For $\beta = 0.85$ the range extends roughly from 0.12 GV/m to 0.5 GV/m and is marked in Fig. 1 with green area. Near the end of the range the overall degree of coherence of the F beam increases slightly which is followed by a notable decrease in $\bar{\mu}$ of the SH beam. The above features can be explained by considering the behavior of the individual realizations as will be seen shortly. It is also observed that for high $\sqrt{S_0}$ values the output $\bar{\mu}$ of both beams is significantly smaller than that at the entrance facet. As an example, for the F wave with $\beta = 0.85$ the

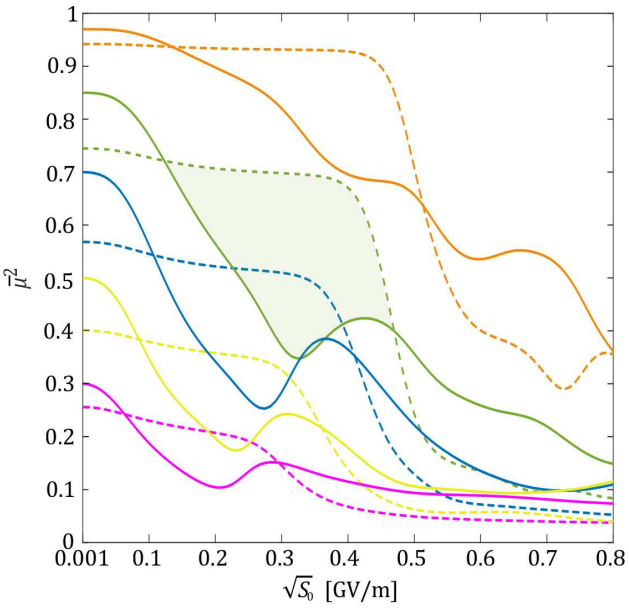

Figure 1. The squared effective degree of coherence of the F (solid lines) and SH (dashed lines) beams propagated through a nonlinear crystal as a function of the incident beam's $\sqrt{S_0}$. The pink, yellow, blue, green, and orange curves correspond, respectively, to $\beta = \{0.3, 0.5, 0.7, 0.85, 0.97\}$ of the incident GSM beam. For the case of $\beta = 0.85$ the region where the SH beam $\bar{\mu}$ is larger than that of the F wave is shaded with green. The various beam and medium parameters are: $\lambda_1 = 0.8$ μm, $w = 40\lambda_1$, $L = 0.5$ mm, $d = 2.0 \times 10^{-12}$ m/V, and $n(\omega_1) = n(\omega_2) = 1.66$.

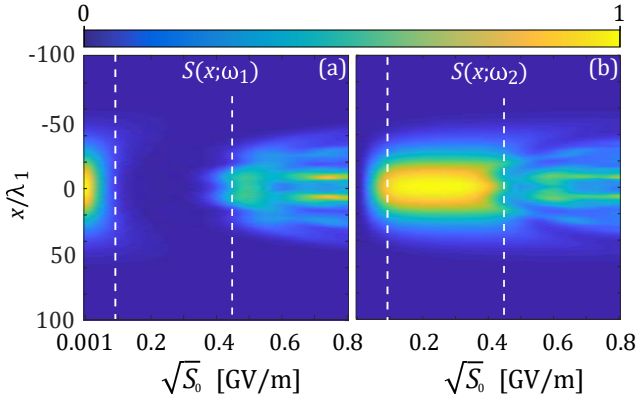

Figure 2. Normalized spectral density distributions of (a) the F field and (b) the SH beam, at the output facet of a nonlinear crystal as a function of $\sqrt{S_0}$. The values at the vertical slices have been normalized by the corresponding S_0. The β value of the incident GSM beam is set to 0.85 and the white dashed lines correspond to the examples discussed in Fig. 4. Other material and field parameters are as in Fig. 1.

overall degree of coherence drops from $\sqrt{0.85} \approx 0.92$ to about $\sqrt{0.08} \approx 0.28$. Hence, interaction with a nonlinear optical material provides a way to render a highly coherent beam into weakly coherent.

The normalized spectral densities of the F and SH beams at the crystal output are shown in Figs. 2(a) and (b) as a function of $\sqrt{S_0}$ in the case of $\beta = 0.85$. Each vertical slice corresponds to a fixed $\sqrt{S_0}$ value. The figures illustrate the coupling of the F-beam and SH-beam energies on transmission. The meaning of the white dashed lines will be explained later. By comparing the spectral density distributions with the overall degrees of coherence of Fig. 1, it is evident that a range of almost constant $\bar{\mu}$ of the SH beam takes place when most of the F-beam energy has been transferred to the SH beam. In contrast, at $0.4 - 0.5$ GV/m, where the abrupt decrease of the degree of coherence of the SH field occurs, the F-wave total output energy is larger than that of the SH field. In general, for a fixed crystal length the output energy oscillates between the F and SH fields as a function of $\sqrt{S_0}$. This behavior is similar to what has been found as a function of the propagation distance in works assessing the efficiency of SHG [3, 19].

To explain the behaviour of the overall degree of coherence of the SH beam we consider an ensemble of incident GSM-beam realizations. Averaging over all realizations produces a Gaussian spectral density distribution. However, individual realizations are not necessarily Gaussian. In particular, when the beam is partially coherent the realizations exhibit random spatial shape possibly with several intensity peaks. Figure 3 shows the spectral density of a typical GSM-beam realization (black dashed lines) as well as the related F-wave (blue solid curves) and SH-wave (red solid curves) realizations in the case of $\beta = 0.5$ for $\sqrt{S_0}$ values of (a) 0.01 GV/m, (b) 0.1 GV/m, and (c) 0.3 GV/m. Note that the GSM-beam realization has the same shape in all three cases. The lower the overall degree of coherence, the more random structure the realizations in general show. For a single realization the SHG is strongest at the locations of high intensity. For a low $\sqrt{S_0}$ value only the strongest intensity peak in a realization is able to contribute significantly to the SH-wave realization whose shape consequently exhibits a peak at this position [red curve in 3(a)]. The spatial locations of these peaks in the SH realizations are highly randomly distributed and represent a field which is less coherent than the F field. This explains why for small $\sqrt{S_0}$ values $\bar{\mu}$ is smaller for the SH beam in Fig. 1.

When $\sqrt{S_0}$ increases more peaks in an F-wave realization can contribute to the SHG and randomness in the SH-field realizations increases [red curve in 3(b)]. This tends to decrease the overall degree of coherence of the SH field as a function of $\sqrt{S_0}$ as observed in Fig. 1. Simultaneously, the peaks in the F-field realizations contributing to the SHG are split into two as the energy in the middle of a peak is transferred to the SH-field realization [blue curve in 3(b)]. This effect increases the number of peaks in the

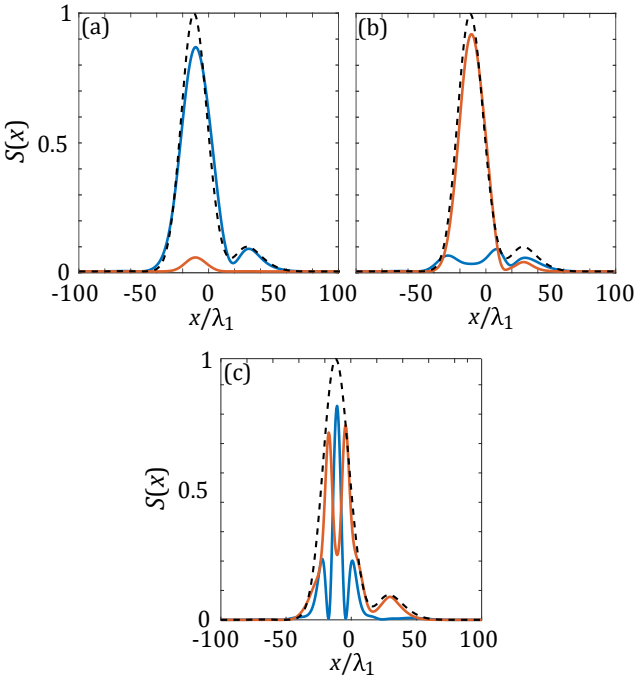

Figure 3. Spectral densities of a typical incident GSM-beam realization (black dashed curve) and the corresponding transmitted F (blue solid curve) and SH (orange solid curve) wave realizations. The incident GSM beam has $\beta = 0.5$ and $\sqrt{S_0}$ equals (a) 0.01 GV/m, (b) 0.1 GV/m, and (c) 0.3 GV/m. All plots have been normalized with S_0.

F-wave realizations and likewise leads to a decreasing trend in $\bar{\mu}$. The abrupt decrease of the SH-field $\bar{\mu}$ occurs when $\sqrt{S_0}$ becomes sufficiently large to induce SHG also in the tail parts of the F-field realizations. Simultaneously, the high amplitude part of the SH realization converts back to the F-wave realization splitting the SH-wave realization. In this case, the SH (and F) realizations show highly peaked (random) structures [red and blue curves in 3(c)]. Similar effects also explain the filamentation of the spectral density distributions as observed in the right-hand sides of Figs. 2(a) and (b) in the case of $\beta = 0.85$. We also remark that multipeaked realizations such as those found by increasing S_0, can likewise be obtained by increasing the crystal length.

Figures 4(a) and (b) show the spectral density distributions of the F field (blue solid curve) and the SH field (orange solid curve) along the white dashed lines located at 0.09 GV/m and 0.45 GV/m, respectively, in Fig. 2. Black dashed lines depict the incident-wave Gaussian spectral density whose peak value is used to normalize all the curves. In Fig. 4(a) the dip in the middle part of the F-beam curve demonstrates the energy transfer to the SH beam which displays a nearly Gaussian shape whereas the filamentation of both beams is visible in (b). Hence, due to the nonlinear optical response of the medium both the F and SH output beams may, at large incident intensities, deviate significantly from a Gaussian shape. Notice also that in the cases of (a) and (b) the overall SH-field degree of coherence is in the flat and rapidly decreasing regions in Fig. 2 (green dashed curve). By comparing the spectral density distributions of the incident and transmitted beams we further observe that the widths are similar for all beams in (a) but in (b) the width of the transmitted F beam is half of that of the SH beam. This suggests that a nonlinear light-matter interaction could be exploited to synthesize a beam with adjustable (narrower) width.

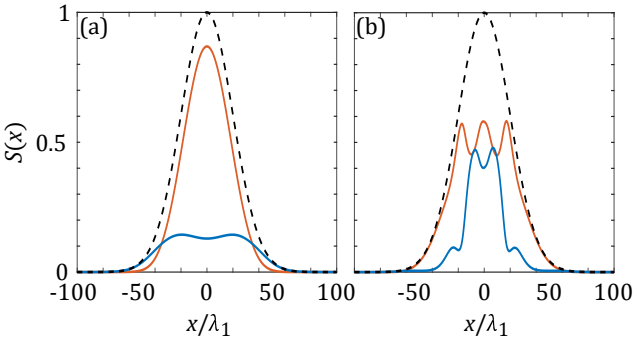

Figure 4. Distributions of the transmitted spectral densities of the F (blue solid curve) and SH (orange solid curve) beams in the cases of (a) $\sqrt{S_0} = 0.09$ GV/m and, (b) $\sqrt{S_0} = 0.45$ GV/m. Black dashed curves show the incident Gaussian spectral density. The situations in (a) and (b), respectively, correspond to the left and right white dashed lines in Figs. 2(a) and (b). All curves have been normalized with S_0.

Figure 5 presents the magnitude of the degree of coherence at the output of a nonlinear crystal for the F beam (left column) and the SH beam (right column). The upper row corresponds to the low amplitude case of $\sqrt{S_0} = 0.09$ GV/m whereas the lower row represents the high amplitude situation with $\sqrt{S_0} = 0.45$ GV/m, which both are also depicted with vertical white dashed lines in Fig. 2. As seen from 5(a), even with a low incident-field amplitudes the degree of spatial coherence of the F beam deviates notably from that of the original GSM beam (which would be a straight diagonal bar but not shown). The origin of this modulation can be traced to the splitting of the F-field realizations as discussed earlier. In contrast, as seen from (b) the SH beam degree of coherence resembles the GSM beam coherence. At high intensities and for both beams the degree of coherence becomes strongly modulated as is visible in (c) and (d). The modulation is particularly strong in the region of high spectral density extending roughly from $-40\lambda_1$ to $40\lambda_1$ [see Figs. 4(a) and (b)]. The above observations suggest that SHG can be employed to alter and control the two-point spatial coherence properties of light beams.

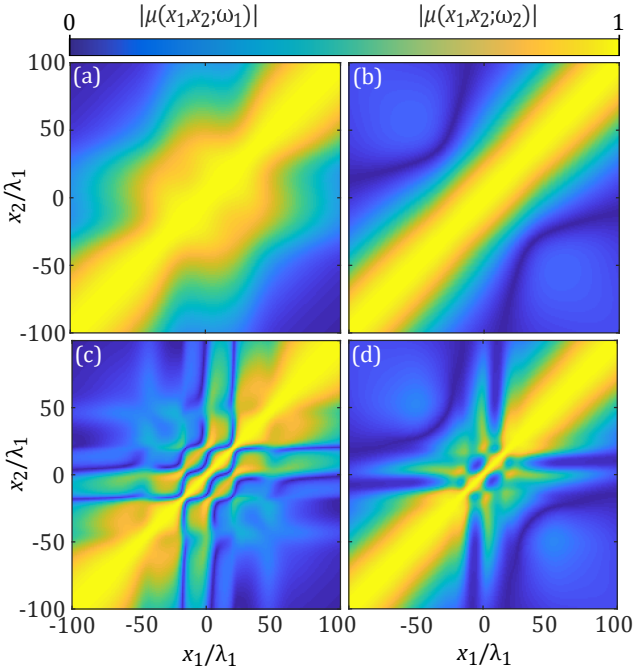

Figure 5. Magnitudes of the degree of coherence of the F beam (left column) and SH beam (right column) at the output facet of a nonlinear crystal for $\beta = 0.85$ of the incident GSM beam. The upper and lower rows correspond to the cases of $\sqrt{S_0} = 0.09$ GV/m and $\sqrt{S_0} = 0.45$ GV/m, respectively, marked with white dashed lines in Fig. 2.

3.2. The phase-mismatched case

Next we assess the situation in which the refractive index is different at different frequencies. We choose $n(\omega_1) = 1.660$ and $n(\omega_2) = 1.661$ which amount to a (dispersive) phase mismatch of $\Delta k = 2k_1 - k_2 = -1.5708 \times 10^4$ rad/m (for collinear components). The other parameters are as in Sec. 3.1. The phase mismatch is expected to reduce the efficiency of the SHG which is clearly visible in Figs. 6(a) and (b) showing the output spectral density distributions for the F and SH beams, respectively, as a function of $\sqrt{S_0}$. In addition, the SHG occurs periodically as function of $\sqrt{S_0}$. Analogous phase-mismatch-induced periodicity of the F- and SH-wave energies but as a function of the propagation distance has been discussed, e.g., in Refs. [3, 19].

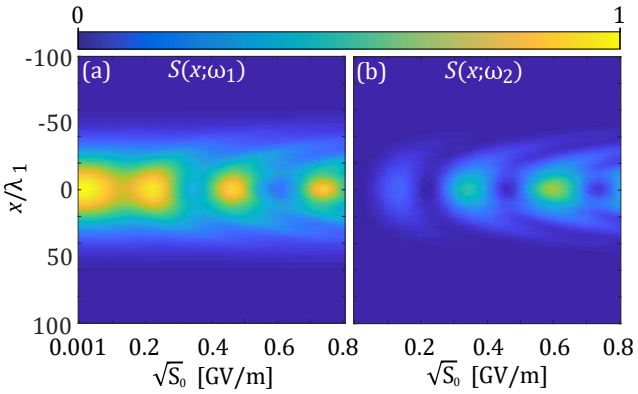

Figure 6. Same as in Fig. 2, but for $n(\omega_1) = 1.660$ and $n(\omega_2) = 1.661$.

The overall degree of coherence as a function of $\sqrt{S_0}$ is presented in Fig. 7 in the cases of $\beta \in \{0.3, 0.5, 0.7, 0.85, 0.97\}$ with pink, yellow, blue, green, and orange lines, respectively. The solid lines refer to the F beam while the dashed lines represent the SH field. For both beams the degree in general decreases with increasing $\sqrt{S_0}$. The mechanism behind this behavior is the same as in the phase-matched case of Fig. 1, i.e., more intensity peaks in the random realizations contribute to SHG while the intensity peaks of F-field realizations are split. Further, by comparing Figs. 6 and 7 we observe that the local maxima of the spectral density coincide with the maxima of the $\bar{\mu}$ curves for both beams. The periodic oscillations in the spectral density and the overall degree of coherence as a function of $\sqrt{S_0}$ originate from the phase mismatch. Similar effects are not present in Figs. 1 and 2.

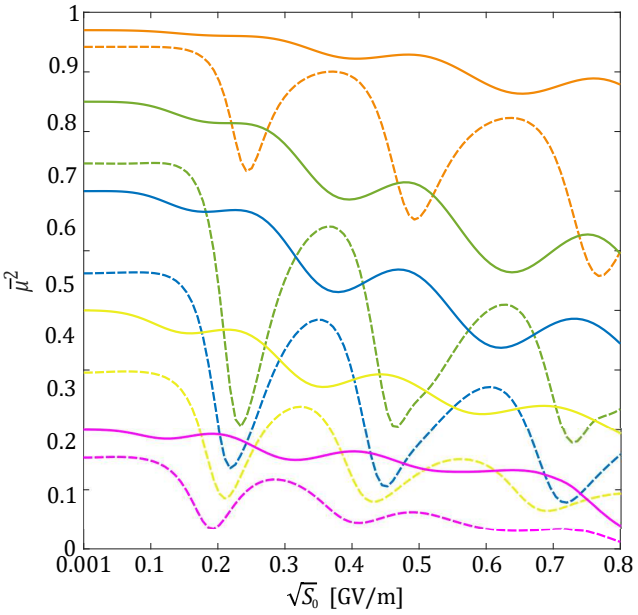

Figure 7. Same as in Fig. 1, but for $n(\omega_1) = 1.660$ and $n(\omega_2) = 1.661$.

4. Conclusions

We analysed the spectral spatial coherence effects in SHG induced by a stationary GSM beam. The overall degrees of coherence of the F and SH fields at the exit facet of a nonlinear crystal were found to decrease significantly with increasing peak intensity of the incident beam. In particular, at strong intensities, a highly coherent GSM beam may generate a weakly coherent SH beam and become highly incoherent itself on propagation. Hence the SHG effect can be used to render a coherent beam into a weakly coherent one. In addition, the coherence properties of both fields may significantly differ from the GSM, especially at high F-wave intensities. In particular, the spectral density distributions of both F and SH waves may show filament structures or the F wave width may be significantly smaller than that of the incident GSM beam. Further, the two-point degree of coherence can be modified to deviate significantly from a Gaussian shape. Propagation in nonlinear medium was performed with the RK and BP methods which led to identical results but the latter was found to be two orders of magnitude faster. The results suggest that the coherence properties of light beams can be tailored and controlled by exploiting a nonlinear material interaction.

Appendix A. Construction of an ensemble of realizations

In this appendix we construct an ensemble of realizations describing a GSM beam. Specifically, we require that the CSD is of the form of Eq. (3) with the modes $\psi_m(x)$ given by the HG functions of Eq. (4). We write a single realization as

$$E_n(x) = \sum_{m=0}^{M-1} \alpha'_{nm}\psi_m(x), \tag{A.1}$$

where M is a sufficiently large number and α'_{nm} are random complex numbers to be determined. Averaging over the ensemble as in Eq. (1) results in

$$W(x_1,x_2) = \sum_{m=0}^{M-1}\sum_{m'=0}^{M-1}\left(\frac{1}{N}\sum_{n=0}^{N-1}\alpha'^{*}_{nm}\alpha'_{nm'}\right) \times \psi^*_m(x_1)\psi_{m'}(x_2), \tag{A.2}$$

where we assumed that the ensemble contains N realizations. Theoretically both N and M should approach infinity but in practise the summations have to be cut as we have done. For Eq. (A.2) to coincide with the CSD of a GSM the following must hold

$$\frac{1}{N}\sum_{n=0}^{N-1}\alpha'^{*}_{nm}\alpha'_{nm'} = \alpha_m\delta_{mm'}, \tag{A.3}$$

where α_m is the modal coefficient given in Eq. (5) and $\delta_{mm'}$ is the Kronecker delta function. We may set

$$\alpha'_{nm} = \sqrt{\alpha_m}\exp(i\phi_{nm}), \tag{A.4}$$

where ϕ_{nm} is a random phase uniformly distributed within the interval $[0, 2\pi]$. Equations (A.3) and (A.4) therefore imply

$$\frac{1}{N}\sum_{n=0}^{N-1}\exp[i(\phi_{nm'} - \phi_{nm})] = \delta_{mm'}. \tag{A.5}$$

Next we introduce the phase matrix

$$\boldsymbol{\phi} = \begin{pmatrix} \exp(i\phi_{00}) & \dots & \exp[i\phi_{0(M-1)}] \\ \exp(i\phi_{10}) & \ddots & \\ \vdots & & \\ \exp[i\phi_{(N-1)0}] & & \exp[i\phi_{(N-1)(M-1)}] \end{pmatrix}, \tag{A.6}$$

whose rows represent individual realizations and columns are mutually orthogonal vectors if M is infinitely large. However, since M is finite we employ the Gram-Schmidt method to render them orthonormal. This then leads to a matrix

$$\mathbf{C} = \begin{pmatrix} c_{00} & \dots & c_{0(M-1)} \\ c_{10} & \ddots & \\ \vdots & & \\ c_{(N-1)0} & & c_{(N-1)(M-1)} \end{pmatrix}, \tag{A.7}$$

whose columns are orthonormal vectors and satisfy

$$\frac{1}{N}\sum_{n=0}^{N-1} c^*_{nm}c_{nm'} = \delta_{mm'}. \tag{A.8}$$

We then set

$$\alpha'_{nm} = \sqrt{\alpha_m}c_{nm}, \tag{A.9}$$

which via Eq. (A.1) generates an ensemble of random realizations that represents a GSM beam. We point out that, e.g., in Refs. [8–10, 12] the above orthonormalization procedure was not employed and hence the resulting CSD may not accurately represent a GSM beam.

Appendix B. Runge–Kutta method

Below we describe the main points of the RK propagation method. We invoke the envelope representation of the field as $E_j(x,z) = A_j(x,z)\exp(ik_jz)$ and for expressing the required formulas we introduce a new variable $A'_j(x,z) = \partial_z A_j(x,z)$ with $\partial_z = \partial/\partial_z$, $j \in (1,2)$. This allows us to split the second-order z derivatives in Eqs. (10) and (11) into four first-order derivatives leading to

$$\partial_z A_1(x,z) = A'_1(x,z), \tag{B.1}$$

$$\partial_z A'_1(x,z) = -4\frac{d\omega_1^2}{c^2}A^*_1(x,z)A_2(x,z)\exp(-i\Delta kz) - i2k_1A'_1(x,z) - \partial_{xx}A_1(x,z), \tag{B.2}$$

$$\partial_z A_2(x,z) = A'_2(x,z), \tag{B.3}$$

$$\partial_z A'_2(x,z) = -2\frac{d\omega_2^2}{c^2}A^2_1(x,z)\exp(i\Delta kz) - i2k_1A'_2(x,z) - \partial_{xx}A_2(x,z), \tag{B.4}$$

where $\partial_{xx} = \partial^2/\partial x^2$ and $\Delta k = 2k_1 - k_2$ are the spatial second-order derivative and the phase mismatch, respectively. The set of Eqs. (B.1)–(B.4) can be integrated with respect to z by employing the RK algorithm [20]. When using an ordinary differential equation solver one needs to perform the spatial second order derivations numerically on every integration step. We also employ a nonlinear coordinate transformation [21] to prevent the reflections from the calculation window boundaries.

Appendix C. Beam-propagation method

Next we outline the BP method [22] for field propagation in a nonlinear medium. The solutions for the homogeneous versions of Eqs. (10) and (11) can be written using the angular-spectrum representation as [23]

$$E_j(k_{xj},z) = \frac{1}{2\pi}\int_{-\infty}^{\infty}E_j(x,z)\exp(-ik_{xj}x)\mathrm{d}x, \tag{C.1}$$

$$E_j(x,z) = \int_{-\infty}^{\infty} E_j(k_{xj},z_0) \times \exp(ik_{xj}x + ik_{zj}\Delta z)\mathrm{d}k_{xj}, \quad \text{(C.2)}$$

where $j \in (1,2)$ and k_{xj} is the spatial frequency, i.e., the wave vector x component, and $\Delta z = z - z_0$ is the propagation step from an arbitrary reference plane at z_0 to z. The z component of the wave vector is $k_{zj} = (k_j^2 - k_{xj}^2)^{1/2}$ for $j \in (1,2)$. To find an expression when the source terms (right-hand sides) are included in Eqs. (10) and (11), we assume that within a small propagation distance Δz the nonlinear polarization changes linearly and its spatial spreading is negligible. Consequently, we may use the slowly-varying envelope approximation (SVEA) [3,24] and write

$$\nabla^2 E_j(x,z) + k_j^2 E_j(x,z) \approx i2k_j\partial_z A_j(x,z), \quad \text{(C.3)}$$

where we have denoted the slowly varying envelope by $A_j(x,z)$, $j \in (1,2)$. We neglected the phase terms $\exp(ik_{zj}z)$ in Eq. (C.3) since the aim is to use the angular-spectrum representation for the field $E_j(x,z)$ that includes the phase. Equating the right-hand side of Eq. (C.3) with those of Eqs. (10) and (11), integrating from z_0 to z, rearranging and combining with Eq. (C.2) yields

$$\int_{-\infty}^{\infty} E_1(k_{x1},z_0)\exp[i(k_{x1}x + k_{z1}\Delta z)]\mathrm{d}k_{x1} = E_1(x,z_0) + \frac{2id\omega_1^2}{k_1c^2}E_1(x,z_0)E_2^*(x,z_0)\Delta z, \quad \text{(C.4)}$$

$$\int_{-\infty}^{\infty} E_2(k_{x2},z_0)\exp[i(k_{x2}x + k_{z2}\Delta z)]\mathrm{d}k_{x2} = E_2(x,z_0) + \frac{id\omega_2^2}{k_2c^2}E_1^2(x,z_0)\Delta z. \quad \text{(C.5)}$$

Above, the F and SH fields in the z_0 plane are known and using Eq. (C.1), one can construct, by employing the FFT, an iterative method for the propagation of the coupled fields.

We tested the numerical methods presented in Appendices B and C by propagating a deterministic Gaussian beam whose width and peak amplitude are $w_0 = 20\lambda_1$ and $A_1(0,0) = 1 \times 10^9$ V/m, respectively, through a second-order nonlinear crystal with the coupling constant $d = 2.0 \times 10^{-13}$ m/V and thickness $L = 1$ mm. In a plane-wave model the chosen peak amplitude corresponds to the power of 100 GW/cm^2 which is easily achieved, e.g., with picosecond pulsed lasers. Such long pulses can be regarded stationary conforming with the assumptions of this work. With 600 and 20000 sampling points in the x and z directions, respectively, the calculation times were 165.5 s (RK) and 0.7 s (BP). Therefore, we may consider the BP method two orders of magnitude faster than the RK technique. Figure C1(a) shows the F and SH waves after propagation in the medium. The incident beam profile is shown with black dashed line whereas solid lines present, respectively, the F (red) and the generated SH (yellow) beams calculated with the RK method. The corresponding spectral densities obtained with the BP method are displayed with purple (F) and green (SH) dashed lines. The results are, to a good accuracy, identical.

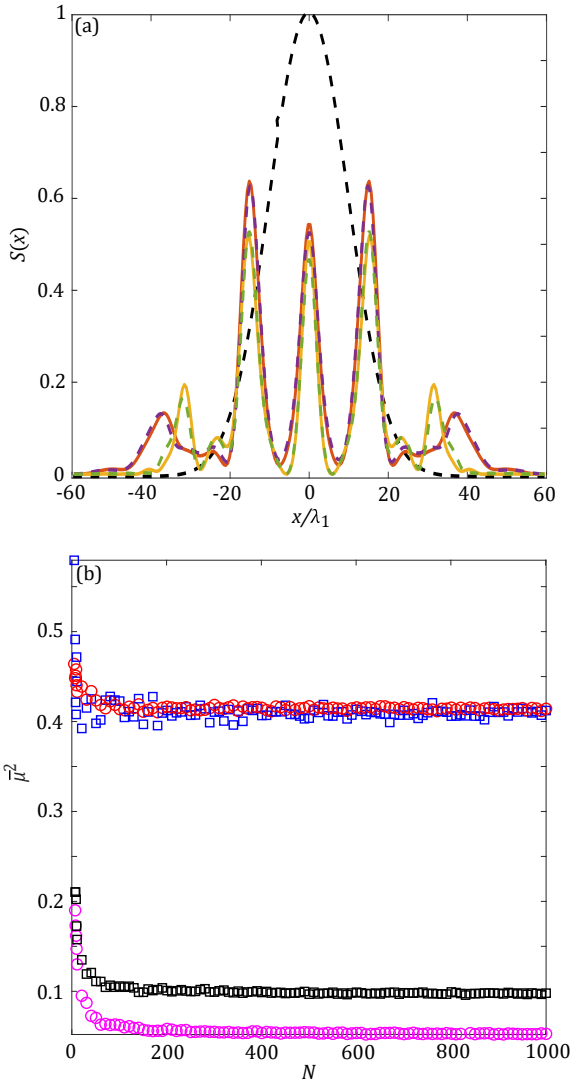

Figure C1. (a) Comparison of the RK and BP methods. Spectral density distributions are shown for the F and SH waves at the output facet of a nonlinear crystal calculated with the RK method [red (F) and yellow (SH) solid lines] and the BP method [purple (F) and green (SH) dashed lines]. The black dashed curve illustrated the incident beam. (b) The squared overall degree of spatial coherence for the F (squares) and SH (circles) waves as a function on the number of realizations. The red and blue symbols denote the case when the initial GSM beam has $\beta = 0.85$, while black and magenta correspond to an incident beam of $\beta = 0.3$. In both cases, the incident beam's average amplitude is 0.45 GV/m.

Appendix D. Convergence arguments

In this appendix we assess the convergence of the results by considering the influence of the number of realizations in an ensemble. As a quantitative measure we employed the overall degree of coherence squared whose values at the nonlinear crystals's exit facet are shown in Fig. C1(b) as a function of the number of realizations. The squares and circles refer to the F and SH waves, respectively, with blue and red colors associated with an incident beam of $\beta = 0.85$, whereas black and magenta represent the situation of $\beta = 0.3$. The incident average amplitude corresponds to the high-intensity case of 0.45 GV/m, which is numerically challenging since both field distributions decompose into narrow filaments. However, in all cases we observe that the overall degree of coherence does not significantly change if the number of realizations exceeds, say, three hundred.

Acknowledgements

Academy of Finland (projects 285880, 308393, and 310511). This work is part of the Academy of Finland Flagship Program, Photonics Research and Innovation (PREIN, project 320166).

References

[1] Mandel L and Wolf E 1995 *Optical Coherence and Quantum Optics* (Cambridge: Cambridge University Press)
[2] Korotkova O 2014 *Random Light Beams: Theory and Applications* (Boca Raton: CRC Press)
[3] Boyd R W 2008 *Nonlinear Optics* 3rd ed (Amsterdam: Elsevier)
[4] Agrawal P A 1995 *Nonlinear Fiber Optics* 2nd ed (San Diego: Academic Press)
[5] Zubairy M S and McIver J K 1987 Second-harmonic generation by a partially coherent beam *Phys. Rev. A* **36** 202–6
[6] Ji L *et al.* 2019 High-efficiency second-harmonic generation of low-temporal-coherent light pulse *Opt. Lett.* **44** 4359–62
[7] Cai Y and Peschel U 2007 Second-harmonic generation by an astigmatic partially coherent beam *Opt. Express* **15** 15480–92
[8] Pyragaite V, Stabinis A and Piskarskas A 2012 Frequency spectrum of second-harmonic radiation exited by a Gaussian Schell-model beam *Phys. Rev. A* **86** 033812
[9] Stanislovaitis P, Narmontas A, Pyragaite V and Smilgevičius V 2014 Generation of a second-harmonic beam from incoherent conical beams *Phys. Rev. A* **89** 043821
[10] Pyragaite V, Smilgevičius V, Butkus R, Stabinis A and Piskarskas A 2013 Conversion of broadband incoherent pump to narrowband signal in an optical parametric amplifier *Phys. Rev. A* **88** 023820
[11] Stockman M I, Bergman D J, Anceau C, Brasselet S and Zyss J 2004 Enhanced second-harmonic generation by metal surfaces with nanoscale roughness: nanoscale dephasing, depolarization, and correlations *Phys. Rev. Lett.* **92** 057402
[12] Lajunen H, Torres-Company V, Lancis J, Silvestre E and Andrés P 2010 Pulse-by-pulse method to characterize partially coherent pulse propagation in instantaneous nonlinear media *Opt. Express* **18** 14979–91
[13] Genty G, Surakka M, Turunen J and Friberg A T 2010 Second-order coherence of supercontinuum light *Opt. Lett.* **35** 3057–9
[14] Halder A, Jukna V, Koivurova M, Dubietis A and Turunen J 2019 Coherence of bulk-generated supercontinuum *Phot. Res.* **7** 1345–53
[15] Närhi M, Turunen J, Friberg A. T. and Genty G 2016 Experimental measurement of the second-order coherence of supercontinuum *Phys. Rev. Lett.* **116** 243901
[16] Ding C, Koivurova M, Setälä T, Turunen J and Friberg A T 2019 Spectral invariance and scaling law for nonstationary optical fields *Phys. Rev. A* **101** 033808
[17] Bastiaans M J 1984 New class of uncertainty relations for partially coherent light *J. Opt. Soc. Am. A* **1** 711–15
[18] Blomstedt K, Setälä T and Friberg A T 2007 Effective degree of coherence: general theory and application to electromagnetic fields *J. Opt. A: Pure Appl. Opt.* **9** 907–19
[19] Armstrong J A, Bloembergen N, Ducuing J and Pershan P S 1962 Interactions between light waves in a nonlinear dielectric *Phys. Rev.* **127** 1918–39
[20] Butcher J C 2016 *Numerical Methods for Ordinary Differential Equations* 3rd ed (Chichester: John Wiley & Sons)
[21] Hugonin J P and Lalanne P 2005 Perfectly matched layers as nonlinear coordinate transforms: a generalized formalization *J. Opt. Soc. Am. A* **22** 1844–49
[22] Feit M D and Fleck J A 1978 Light propagation in graded-index optical fibers *Appl. Opt.* **17** 3990–8
[23] Goodman J W 2005 *Introduction to Fourier Optics* 3rd ed (Englewood: Roberts & Company)
[24] Trebino R 2000 *Frequency-Resolved Optical Grating: the Measurement of Ultrashort Laser Pulses* (Boston: Springer)